

Sea Ice Concentration Estimation Techniques Using Machine Learning

A Deep Learning approach to estimating sea ice concentrations
in the Southern hemisphere



Presented by:
Muneeb Bray

Prepared for:
Dept. of Electrical and Electronics Engineering
University of Cape Town

Submitted to the Department of Electrical Engineering at the University of Cape Town
in partial fulfilment of the academic requirements for a Bachelor of Science degree in
Electrical Engineering

November 11, 2020

Abstract

The current state of affairs in sea ice concentration estimations are aimed at producing numerical models calibrated in the Northern hemisphere. These models utilise the behaviour and features present in sea ice regions and produce somewhat biased predictions. Remote-sensing instrumentation such as passive microwaves and synthetic aperture radar has the capabilities to provide a useful set of data that can be implemented with a Machine Learning approach. Deep Learning is a subset of Machine Learning and coupled with the remote-sensed data, it stands to deliver a promising solution to the problem presented. An engineering investigation will take place that employs the use of the scientific method with relevant research substantiating the results. Google Colab is used for all coding aspects of the investigation and provides the platform for which the results are produced. The code and some of the models and data sets are uploaded to a GitHub repository and available for viewing purposes.

GitHub Repository:

<https://github.com/MuneebBray/UCT-SIC>

Contents

1	Introduction	1
1.1	Background to the study	1
1.2	Objectives of this study	2
1.2.1	Problems to be investigated	2
1.2.2	Purpose of the study	2
1.3	Scope and Limitations	3
1.4	Plan of development	4
2	Literature Review	6
2.1	Analysing Sea Ice Information	6
2.2	Data Sources	8
2.2.1	National Snow and Ice Data Center (NSIDC)	8
2.2.2	Copernicus Marine Environment Monitoring Service (CMEMS) .	9
2.2.3	Copernicus Open Access HUB	9
2.3	Machine Learning Methods	10

2.3.1	Multilayer Perceptron (MLP)	11
2.3.2	Long and Short-Term Memory (LSTM)	11
2.3.3	Fully Convolutional Neural Network (FCNN)	12
2.3.4	UNet	12
2.3.5	DenseNet	12
3	Requirement Analysis	13
3.1	User Requirements	13
3.2	Functional Requirements	14
3.3	Specifications	15
3.4	Acceptance Tests Protocol	16
4	Data Sources	18
4.1	Data Source Selection	18
4.1.1	Satellite Image Data	18
4.1.2	Ground Truth Image Data	19
4.2	Data Acquisition	19
4.2.1	Copernicus SAR Images	19
4.2.2	OSI-401-b SIC Images	20
4.3	Data Pre-processing	20
4.4	Data Curation	21

4.5	Summary of Data Sets	23
4.6	Analysing Errors in Data Sources	24
4.6.1	Pass Direction Mislabelling	24
4.6.2	Error Correction	25
5	Neural Networks	26
5.1	Convolutional AutoEncoder Network	26
5.1.1	Implementing the AutoEncoder for SIC Estimations	27
5.2	LinkNet	27
5.2.1	Implementing LinkNet for SIC Estimations	29
6	Model Training and Evaluation	30
6.1	Model Naming Convention	30
6.2	Model Training Process	31
7	Results	33
7.1	Model Performance	33
7.1.1	Mean Absolute Error Losses	33
7.1.2	Mean Square Error Losses	36
7.2	Comparing Model Predictions	37
7.2.1	Convolutional AutoEncoder vs. LinkNet	37
7.2.2	UW MAE vs. UB MSE	40

7.2.3	Southern Hemisphere (Freezing)	41
7.2.4	Southern Hemisphere (Melting)	43
7.3	Correcting Discontinuities within the Predictions	44
7.4	Acceptance Tests	46
8	Discussion	48
8.1	LinkNet compared to previous Neural Networks	48
8.2	The Inclusion of Melting and Freezing Cycles	48
8.3	The Lack of Data Augmentation Techniques	49
8.4	The Approach to Transfer Learning	49
8.5	User Requirements	50
9	Conclusions	51
10	Recommendations	52
10.1	Alternative Neural Networks	52
10.2	Transfer Learning	52
10.3	Increase Image Dimension	53
10.4	Alternative Data Sources	53
A	Neural Network Predictions	56
A.1	AutoEncoder Predictions	56
A.1.1	Arbitrary Locations	56

A.2 LinkNet Predictions	57
A.2.1 Arbitrary Locations	57
A.2.2 Specific Locations in the Antarctic Region	58

List of Figures

2.1 Comparison of the maximum and minimum SIE of the Antarctic region during its the peak of each season. Source: Adapted from [2]	7
4.1 The resampled SAR image presented with its corresponding SIC and uncertainty label.	21
4.2 This SAR image is selected in the data curation process as it contains a variation of 0.0553 which is above the minimum threshold of 0.05. It Also displays a histogram of the concentration distribution within the SAR image.	22
4.3 This SAR image is disregarded in the data curation process as it contains a variation of 0.0414 which is below the minimum threshold of 0.05. It Also displays a histogram of the concentration distribution within the SAR image.	22
4.4 This SAR image was obtained during the satellites ASCENDING pass and displays the correct image footprint as well as the rotation error.	24
4.5 A series of images retrieved from the satellite mapping the satellites trajectory of ingestion.	25
5.1 A diagram illustrating the connections within the AutoEncoder architecture.	27
5.2 A diagram illustrating the connections within the LinkNet architecture. Source: Adapted from [11].	28

7.1 A LinkNet model trained and tested on Southern hemisphere data during its freezing period. The figure contains 4 images, the input to the model, the prediction produces by the model, the ground truth image for which the prediction is compared to and the uncertainty label obtained from the OSI-410-b product.	38
7.2 An AutoEncoder model trained and tested on Southern hemisphere data during its freezing period. The figure contains 4 images, the input to the model, the prediction produces by the model, the ground truth image for which the prediction is compared to and the uncertainty label obtained from the OSI-410-b product.	38
7.3 A LinkNet model trained and tested on Northern hemisphere data during its freezing period. The figure contains 4 images, the input to the model, the prediction produces by the model, the ground truth image for which the prediction is compared to and the uncertainty label obtained from the OSI-410-b product.	39
7.4 An AutoEncoder model trained and tested on Northern hemisphere data during its freezing period. The figure contains 4 images, the input to the model, the prediction produces by the model, the ground truth image for which the prediction is compared to and the uncertainty label obtained from the OSI-410-b product.	40
7.5 A LinkNet model trained and tested on Southern hemisphere data during its melting period using UW MAE as the loss. The figure contains 4 images, the input to the model, the prediction produces by the model, the ground truth image for which the prediction is compared to and the uncertainty label obtained from the OSI-410-b product.	40
7.6 A LinkNet model trained and tested on Southern hemisphere data during its melting period using UB MSE as the loss. The figure contains 4 images, the input to the model, the prediction produces by the model, the ground truth image for which the prediction is compared to and the uncertainty label obtained from the OSI-410-b product.	41

7.7	A LinkNet model trained on Southern hemisphere data during its melting period and tested on Southern hemisphere data during its freezing period. The figure contains 4 images, the input to the model, the prediction produces by the model, the ground truth image for which the prediction is compared to and the uncertainty label obtained from the OSI-410-b product.	42
7.8	A LinkNet model trained on Northern hemisphere data during its freezing period and tested on Southern hemisphere data during its freezing period. The figure contains 4 images, the input to the model, the prediction produces by the model, the ground truth image for which the prediction is compared to and the uncertainty label obtained from the OSI-410-b product.	42
7.9	A LinkNet model trained and tested on Southern hemisphere data during its melting period using UW MAE as the loss. The figure contains 4 images, the input to the model, the prediction produces by the model, the ground truth image for which the prediction is compared to and the uncertainty label obtained from the OSI-410-b product.	43
7.10	A LinkNet model trained on Northern hemisphere data during its freezing period and tested on Southern hemisphere data during its melting period. The figure contains 4 images, the input to the model, the prediction produces by the model, the ground truth image for which the prediction is compared to and the uncertainty label obtained from the OSI-410-b product.	44
7.11	A LinkNet model trained and tested on Southern hemisphere data during its freezing period. The figure contains 4 images, the input to the model, the prediction produces by the model, the ground truth image for which the prediction is compared to and the uncertainty label obtained from the OSI-410-b product.	45
7.12	A LinkNet model trained on Southern hemisphere data during its melting period and tested on Southern hemisphere data during its freezing period. The figure contains 4 images, the input to the model, the prediction produces by the model, the ground truth image for which the prediction is compared to and the uncertainty label obtained from the OSI-410-b product.	45

List of Tables

3.1	Table representing Requirements Specifications.	13
3.2	Table representing Functional Requirements	14
3.3	Table representing Requirements Specifications	15
3.4	Table representing Acceptance Tests Protocol	16
4.1	Table representing a summary of the data sets used to train the models . .	23
7.1	A summary of the Mean Absolute Error of each model during the training and testing phase. The losses highlighted in green represent the best testing loss for that specific loss variant of its respective section (freezing/melting). The losses highlighted in blue represent the best overall testing loss for each section (freezing/melting)	34
7.2	A summary of the Mean Square Error of each model during the training and testing phase. The losses highlighted in green represent the best testing loss for that specific loss variant of its respective section (freezing/melting). The losses highlighted in blue represent the best overall testing loss for each section (freezing/melting)	36
7.3	The outcomes of the Acceptance Tests derived at the beginning of the investigation	46

Chapter 1

Introduction

1.1 Background to the study

Sea ice concentrations (SIC) in the Arctic and Antarctic regions are an important aspect of nautical navigation and climate research for climatologists. Monitoring these wide regions require large and accurate data sets with high spatio-temporal resolutions. There are various free and reliable sources of these data sets available for research purposes. The National Snow and Ice Data Center (NSIDC) as well as the Copernicus Marine Environment Monitoring Service (CMEMS) have been used in past research to analyse SIC in both the Northern and Southern Hemispheres. Although these data sets are available, the amount of data acquired in the Southern Hemisphere is significantly less than in the Northern Hemisphere. This is a result of the high water vapour content in the atmosphere of the Southern region, which inhibits the Passive Microwaves (PMW) instrumentation from acquiring the SIC data. Synthetic Aperture Radar (SAR) has the capability to penetrate the atmosphere and provide image data that can be used in a machine learning model to produce SIC estimates.

Predominantly, numerical models have been at the forefront when measuring SIC data. However, these models require accurate data sets within a specified region of interest. And due to the lesser available data in the Antarctic, numerical models based on Northern regional data have been applied to the Southern region. This implementation has performed to no avail and is attributed to the significant differences in feature characteristics of the respective regions, such as winds, storms, melting & freezing periods, atmospheric conditions etc.

1.2. OBJECTIVES OF THIS STUDY

The concept of Machine Learning methods for concentration mapping have recently been introduced, and provides an effective tool that can be applied to the situation mentioned above. Machine learning methods are able to recognise patterns based on ground truth data for a specific region & time and produce a SIC estimation with high spatio-temporal resolution. Therefore, the application of Machine learning methods for concentration mapping poses a plausible solution to the minimal sea ice data in the Southern region compared to the Northern region.

1.2 Objectives of this study

1.2.1 Problems to be investigated

We already know from past research that Machine Learning methods can be used to produce SIC estimates with reasonable accuracy. But there is a question of whether the studies performed were able to utilise all the information available, if the information used was effective and reliable, and if there were any data sources or information overlooked in the data acquisition and model training & evaluation process.

There is also a question if the previous Neural Network architectures were optimised to give the best results and if there are any newer/improved Neural Network architectures based on Image Segmentation available to be adapted for SIC estimations to images with high spatio-temporal resolutions.

A useful comparison tool could be developed to compare the SIC estimates obtained from the Neural Network models and the PMW sourced data. This tool also would allow the user to search any coordinate, and the model would produce a SIC estimate within a given accuracy.

1.2.2 Purpose of the study

Given that countless researchers observing and monitoring polar sea ice, they would certainly pose questions regarding the validity of the data sets acquired from PMW instrumentation, especially in Southern regions such as the Antarctic. Applying Machine Learning methods specific to SIC estimation in the Antarctic provides an extra layer of validity giving scientists and researchers the ability to explore new findings hidden in the

poorly documented Antarctic region.

There are numerous features pertaining to SIC's in both the Southern and Northern polar regions. This investigation aims to utilise one of these features and develop a SIC estimation model calibrated for the Southern hemisphere.

The following Neural Network architectures were implemented in past research and have shown acceptable results: A Multilayer Perceptron Network (MLP), Long-Short Term Memory Network (LSTM), a simple convolution neural network (CNN), UNet, and DenseNet. These will provide context as to how the results of this investigation are to fit within the gap present in SIC estimation models using Machine Learning.

1.3 Scope and Limitations

In the investigation conducted prior to the experimentation process, the literature review was produced which aided in refining the project scope limitations.

The project entails obtaining large data sets over a long period of time. These data sets contain information regarding SIC's (PMW) obtained from the OSI-SAF product provided by CMEMS and satellite images (SAR) obtained from the SENTINEL-1 satellite provided by Copernicus Open Access Hub. These data sets were acquired during specific seasonal cycles of when freezing and melting periods occur. These cycles describe the changing of the sea ice extent throughout the investigation.

The project does not include factors affecting SIC's such as storm conditions, sea ice drift, sea ice thickness, winds, ocean currents, and temperature. These factors mentioned all play a role in the rate of growth of SIC's, but unfortunately were not able to be implemented into a Machine Learning model used to produce SIC estimations. The reason for this was that these factors often were not able to be shaped/transformed into the same data type as the output that was required for the Neural Network model to produce.

The investigation was performed in tandem with 3 additional final year BScEng (Electrical Engineering) courses for the first half of the second semester of my final year. The project then became the primary focus of my semester in the second half of the semester. Progress was initially hampered by the other courses on the sidelines, which inhibited me from fully delving and familiarising myself with the research.

Google Colab accompanied by a Google Drive was also used to execute all the coding aspects of the project including data acquisition, Neural Network implementation, and designing the search interface incorporating the trained models. These platforms gave rise to various challenges that required time to find a workaround solution. With better time management it would provide a platform to conduct the investigation backed by extensive research with minimal setbacks.

1.4 Plan of development

The plan presented below provides a detailed sequence of events which elaborates each step of the conduction of this investigation. The research conducted prior to the execution of the methodology is presented in the literature review.

Stage 1: This stage introduces the problem to be researched throughout the investigation and outlines what will be included and excluded. A project objective is defined and the purpose of the study is presented.

Stage 2: The second stage presents the Literature Review and identifies the gap in which this investigation is situated compared to previous research. It details the necessary information that this investigation is based on and familiarises the reader with the relevant information.

Stage 3: The Requirement Analysis is presented in this stage and elaborates on a specific set of functions that will be assessed at a later stage to determine the project success. These requirements are developed based on the research presented in the Literature Review and evaluated throughout the conduction of the investigation.

Stage 4: This stage details the process of data source selection and acquisition. The entirety of the data pre-processing is explained as well as the workaround solution to errors present in this downloaded data. The data is labelled and prepared for use in the next stage of the investigation.

Stage 5: In this stage, the Neural Networks are defined, created and the Python libraries specified. Each Neural Network choice is chosen based on the Literature Review and adapted to produce SIC estimations.

Stage 6: This stage involves detailing the functions and libraries used in the training

1.4. PLAN OF DEVELOPMENT

process for the models of each network as well as defining the model naming convention.

Stage 7: The results stage analyses all the performances and predictions of each model while explaining specific decisions made in the experimental process. It provides critical analysis that draws conclusions based on the outline in the User Requirements. The Acceptance Tests are performed and assessed if each test passes the requirement.

Stage 8: The discussion stage explores the findings obtained throughout the investigation and elaborates on specific decisions made in the beginning stages of the project.

Stage 9: This stage essentially summarises what was achieved in this investigation and draws conclusions based on the evidence found pertaining to any initial theories.

Stage 10: Lastly, a list of recommendations are presented that are in line with the goal of this investigation. It provides a launch platform for further research in the field of SIC estimation by listing constructive improvements to be made. These recommendations are abstract and purely based on the research conducted.

Chapter 2

Literature Review

In our attempt to develop a tool that has the ability to aid scientists and researchers in filling the gap of SIC data in the Southern Hemisphere, we have to identify the root issue and familiarise ourselves with the idea of SIC's and the research conducted prior to this investigation.

Firstly, let's take deep dive into the differences separating the Arctic and our region of focus, the Antarctic. Both these large masses of ice share many similarities as well as differentiations that separate the two. They are both situated on either end of the Earth's polar regions and forms a large percentage of the Earth's cryosphere. While this may seem a similarity to some, this geographical position in fact plays an important role in dictating the environments of each mass of land.

The Antarctic region is known to have one of the largest variation of its geographical footprint throughout history. This is one of the reasons pertaining to the complexity of obtaining valid and accurate data with high spatio-resolutions.

2.1 Analysing Sea Ice Information

Sea ice is essentially frozen seawater. In this frozen state, the sea ice is less dense than the seawater itself and tends to float above the sea level. Approximately 15% of the Earth's oceans are covered by sea ice and is slowly decreasing due to the effects of climate change, as these polar regions are the most sensitive to the changes [1].

2.1. ANALYSING SEA ICE INFORMATION

For the purpose of this investigation, the Northern and Southern polar regions will be focused. It is apparent in the Data Sources section that there is a significant deficit in the data available in the Southern polar region. This provides a challenge for researchers with the intention of analysing the region specifically in climate change. With the purpose of this investigation being to develop a SIC estimation model, it provides an opportunity to introduce additional information that may have been overlooked in the past, that can then be utilised to fine-tune the model.

In scouring the resources available, one research paper was found that made use of the seasonal cycles that occur in the Northern and Southern polar regions [7]. However, a majority of the papers focused on deriving models based on daily and averaged monthly SIC data without the addition of an external feature that could improve their models. The seasonal cycles in these regions presents a feature that can potentially benefit the research in this field.

In an investigation conducted by the NASA Earth Observatory [2], it was found that these polar regions, the Arctic and Antarctic, undergo significant changes in its sea ice extent (SIE), with the Antarctic experiencing a more drastic change as seen in Figure 2.1. The SIE is the total area covered by some amount of ice, a cutoff point of 15% SIC is commonly defined by scientists as the minimum threshold of the sea ice edge. Meaning that ice with a concentration lower than 15% is not defined as part of the SIE.

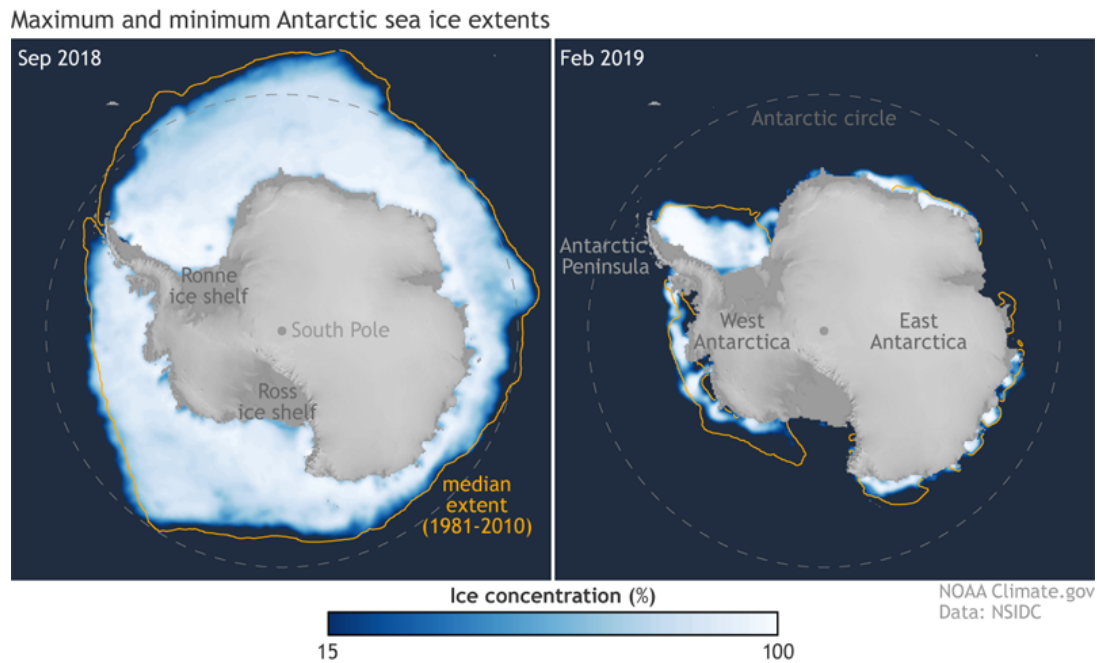


Figure 2.1: Comparison of the maximum and minimum SIE of the Antarctic region during its peak of each season. Source: Adapted from [2]

These peak cycles can be used in the data acquisition process where the SIC images are obtained based around these periods. In theory, applying this concept may improve the SIC model by providing insight into "hidden" features in the data.

2.2 Data Sources

There contains a myriad of data sources across the internet that will allow implementation for a SIC estimation model. These data sources provide extensive data regarding the cryosphere for researchers and scientists such as climatologists to analyse.

In selecting a product to implement, specific criteria has to be met that will allow the SIC estimation model to provide optimal results. The product needs to provide data with a high spatio-temporal resolution. This means that the product is required to deliver information (data sets) that is recent and can be updated for future improvements/research. The spatial resolution aspect of the product requirement aims to provide images for the SIC estimation model with high detail in order to produce accurate estimations.

2.2.1 National Snow and Ice Data Center (NSIDC)

One of these data sources is the NSIDC, the NSIDC manages and distributes scientific data and creates tools for data access so that scientists are able to perform scientific research regarding the cryosphere. The NSIDC contains numerous products providing information regarding sea ice, from sea ice concentrations to sea ice thickness as well as sea ice temperatures.

There are two individual products that were analysed that provide the best data sets in terms of spatio-temporal resolution.

Sea Ice Index, Version 3 provides SIC images in a PNG format covering the Northern and Southern polar regions. These images are sourced with **Special Sensor Microwave Imager / Sounder (SSMIS)** remote sensors. SSMIS is a variation of PMW instrumentation that combines and extends the current imaging and sounding capabilities of previous PMW data sourcing. The product provides a spatial resolution of 25 km x 25 km, and a temporal resolution of 1 day. The images and data are produced in a consistent way that makes the Index time-series appropriate for use when looking at long-term trends in sea

ice cover.

The second product assessed from the NSIDC is the *AMSR-E/AMSR2 Unified L3 Daily 12.5 km*. Like the first product, it provides images in a PNG format covering Northern and Southern polar regions. These images are sourced using **AMSR2**, this instrument measures weak microwave emissions from the Earth's surface and atmosphere and provides accurate measurements of microwave emissions and scattering. The antenna of AMSR2 rotates once every 1.5 seconds and obtains data over a 1450 km swath on the Earth's surface [4]. The product provides the same temporal resolution as the first product (1 day). A spatial resolution of 12.5km x 12.5km provides an improvement to the first product, therefore, is more suited to our requirements.

2.2.2 Copernicus Marine Environment Monitoring Service (CMEMS)

CMEMS provides full, free and open access to data and information related to the global ocean and the cryosphere.

One of the products sourced by CMEMS is acquired by the Ocean and Sea Ice Satellite Application Facility (OSI SAF). OSI-SAF is a member of the European Organisation for the Exploitation of Meteorological Satellites (EUMETSAT) community and provides comprehensive information derived from meteorological satellites at the ocean-atmosphere interface.

OSI-401-b [5] is a product that provides improved SIC images compared to previous OSI-SAF products. The SIC images are obtained via **PMW** radar and provides a temporal resolution of 1 day and a spatial resolution on a grid space of 10km x 10km. One advantage this product has over the NSIDC products is the addition of an uncertainty layer. This uncertainty layer contains values based on the quality of the input data used to generate each concentration pixel value. An implementation of this layer in the SIC estimation model can prevent the model from learning inaccurate labels.

2.2.3 Copernicus Open Access HUB

Copernicus [6] provides open access to various SENTINEL missions such as SENTINEL-1, SENTINEL-2, SENTINEL-3 and SENTINEL-5P. These missions form part of the Copernicus Satellite Constellation Programme conducted by the European Space Agency

(ESA).

The SENTINEL missions are composed of two twin polar-orbiting satellites using multi-sensors to retrieve images of various types. The images can be catered to the user's specific requirements by fine-tuning the search interface embedded in the Copernicus browser.

The *SENTINEL-1* mission focuses on obtaining images day and night using **Synthetic Aperture Radar (SAR)** instrumentation. The use of capturing images via SAR allows the retrieval of images in all weather conditions with high reliability of service. The satellites are able to provide high resolution raw, ground range detected and ocean images. There are 4 modes available to specify the swath size, choosing the swath size inherently affects the spatial resolution. The two modes which could be applied to the SIC estimation model is the Strip Map Mode (SM) and Extra-Wide Swath Mode (EW). SM provides a spatial resolution of 5m x 5m with an 80 km swath, while EW provides a 20m x 40m spatial resolution with a 400 km swath. When considering each mode, the swath size is crucial in obtaining as much data as possible. Therefore each filtering mode has benefits to the SIC estimation model but may hinder results if minimal images are available.

These specifications analysed above suit the requirements to implement into the estimation model and could be a viable means of acquiring the SIC data needed for our research purposes. The choice of data sources will be elaborated in the methodology explaining the optimisation and processing of the chosen data source.

2.3 Machine Learning Methods

A numerical model for SIC estimations is complex to define as it uses a variety of sea ice features to estimate SIC. Features like ice drift and ocean temperature can be used to develop such a model, but these measurements are unpredictable and in turn skew the results of the model, producing a somewhat inaccurate model

In exploring the numerical models of SIC estimation, it is evident that an alternative model would be required for an effective SIC estimation model calibrated to the Southern hemisphere. In recent years Machine Learning methods have been implemented in sea ice monitoring models in order to make up for the lack of data available or correcting existing models.

Machine Learning presents a tool that can provide countless methods of approaching a specific problem. The applications for Machine Learning ranges from object detection implementing Image Segmentation techniques to Speech to Text learning algorithms.

There are numerous pre-trained Neural Network architectures available online that can be applied for general and more common purposes. For example, for concentration mapping, there are not many pre-trained or even aimed at Neural Network architectures available to just import and apply. As this is not a common application for Neural Networks, further research has to be conducted in adapting an existing architecture or perhaps creating an architecture from scratch.

An elaboration of the previous Neural Networks implemented for SIC estimation is presented in the subsection below. These Neural Network architectures are based on two papers that are directly in line with the goals of this investigation [3][7]. MLP and LSTM models in the second paper [7] were tested on monthly data assessing the effect of freezing and melting cycles. The other Neural Networks in [3] produced results based on SAR images at face value without taking into account the period of acquisition.

2.3.1 Multilayer Perceptron (MLP)

An MLP network can also be identified as a feedforward neural network. These types of networks are made up of outer and inner layers where the inner layers are the "hidden" layers. These layers each contain a finite number of neurons with each neuron defined by a weight. These weights are obtained via an iterative process using gradient backpropagation through the layers and inherently optimising the model output. These final models produced a root mean square (RMS) error of less than 10%, which is an indication of high performance.

2.3.2 Long and Short-Term Memory (LSTM)

The LSTM network is a derivation of a standard Recurrent Neural Network. Its learning process is similar to the MLP, where it passes the image through the layers but instead of backpropagating at the end, it backpropagates in specified interim loops between the layers. This network is efficient in learning long term dependencies and provides an alternative approach to SIC estimation models. In the paper presented [7], the LSTM models performed the best in terms of average error performance, while noting that the

performances in the MLP models were not far off.

2.3.3 Fully Convolutional Neural Network (FCNN)

The FCNN is a basic Neural Network that is able to perform image segmentation as well as SIC estimations in the interest of this investigation. This particular Neural Network was implemented in one of the research papers [3] and produced effective results with performances that met the specified requirements.

2.3.4 UNet

The UNet Neural Network provides an architecture that takes advantage of skip connections. It was also created with the intention of performing image segmentation, but it can be adapted to produce an accurate SIC estimation model trained on Northern and Southern hemisphere data. Models trained with this Neural Network produced the best results in terms of testing loss [3]. Therefore a similar Neural Network could be sought out that is based on the UNet structure and adapted for SIC estimations.

2.3.5 DenseNet

The DenseNet Neural Network architecture, unlike the UNet architecture, passes the images through the layers without performing any downsampling and upsampling. In the same research paper as the UNet models [3], the DenseNet models were tested and resulted in the worst performance compared to the other models, even with transfer learning and data augmentation applied. Due to these results, a Neural Network created with a similar architecture was not sought out in the investigation process.

Chapter 3

Requirement Analysis

The following set of requirements and specifications were drawn up based on the findings presented in the Literature Review. It is created with the intention of producing an improved SIC estimation model for the Southern hemisphere region. They provide an overview of the tasks to be completed that would justify the position of the investigation in the gap of SIC estimation techniques.

3.1 User Requirements

The User Requirements presented in Table 3.1 and its subsequent derivations are presented in a top-down approach with the User Requirements outlining the structure.

User Requirements	
ID	Details
U1	Predict a sea ice concentration estimation centred around a specified geographic coordinate.
U2	Predict sea ice concentration estimates with ground truth observations within a desired accuracy range.
U3	Compare sea ice concentration estimation models made in the Arctic and Antarctic.
U4	Provide sea ice concentration estimations based on high resolution data (SAR etc.).

Table 3.1: Table representing Requirements Specifications.

3.2. FUNCTIONAL REQUIREMENTS

There are four User Requirements each detailing a key feature that the SIC estimation model is required to produce. Each User Requirement is labelled and assigned a colour based on achievability (green-yellow-red). Meeting these requirements is essential to the purpose of the investigation and any significant failures would undermine the research conducted during the investigation. The requirements presented are basic ideas in the field of Machine Learning, hence the overall high achievability of each requirement.

3.2 Functional Requirements

The Functional Requirements in Table 3.2 below expand on each User Requirement mentioned above. It details how the investigation pans out in terms of functionality by defining a more clear set of requirements.

Functional Requirements		
Tree	ID	Details
U1	F1	Create a neural network that can predict sea ice concentrations for a given coordinate.
	F2	Provide a functioning software tool (search interface) with an easy-to-use UI that can create ice charts in real time.
U2	F3	Develop a neural network that can perform optimised predictions with a desired accuracy of 90%.
	F4	Use alternative data sources to account for inaccuracies in existing models.
U3	F5	Neural network model needs to be calibrated for both Southern and Northern hemisphere.
	F6	Use alternative techniques to create variation of the minimal data available in the Southern hemisphere.
U4	F7	Input/output dimension of neural network scaled up to accompany high resolution data.
	F8	Sort data retrieved from the source into categories based on valuable information.

Table 3.2: Table representing Functional Requirements

Four of these requirements are not highlighted in green due to them all regarding the performance of the model, which cannot be predicted at this stage.

3.3 Specifications

Specifications			
Tree	ID	Details	
U1	F1	S1	A neural network model (LinkNet) will be trained with labelled ground truth ice charts (OSI-401-b) and used to estimate ice concentration levels at a given coordinate.
	F2	S2	A friendly UI can be designed (in Google Colab) that is simpler to understand with minimal inputs. The ice chart concentration estimations will achieve high spatio-temporal resolution.
U2	F3	S3	Create different neural network models comprised of different training data (Varying regions – Antarctic & Arctic, varying periods – freezing and melting) and choose model with best accuracy.
	F4	S4	Storm patterns, ground & sea temperature, OSI SAF ground truth data etc. to be utilised at a given area to account for breaks/discontinuities in the ice chart estimations.
U3	F5	S5	Training partially on the more accurate Northern hemisphere data, before completing training on data from the Southern hemisphere.
	F6	S6	Seasonal cycles to be implemented in order to increase the number of high-resolution images (obtained from Copernicus Open Access Hub).
U4	F7	S7	The convolutional neural network model (LinkNet) maintains the input dimensionality at the output so it will be able to train a model based on high-resolution SAR images (obtained from Copernicus Open Access Hub).
	F8	S8	Copernicus Open Access Hub can be used to retrieve SAR data at a specific coordinate with the images having a typical pixel spacing of 10 to 40 meters. Not all of these data images will contain enough variation of ice concentrations so it would need to be sorted using an algorithm.

Table 3.3: Table representing Requirements Specifications

The specifications in Table 3.3 define all aspects regarding what needs to be produced or at least explored during the investigation. It details the data sources as well as the Neural Network architectures to be implemented. And also provides a framework that aims to produce improved results that can be built for further research. The specifications mentioned aide in accomplishing what is outlined in the User Requirements as illustrated by the tree table linking each specification to an independent User Requirement in the tree table.

3.4 Acceptance Tests Protocol

Acceptance Tests Protocol								
Tree		ID	Details					
U1	F1	S1	T1	Apply the trained neural network model to a SAR image and make a prediction. Compare the geological footprint of the ground truth image at the coordinate to the prediction. Pass: The geological footprint of the prediction and ground truth image are identical.				
	F2	S2	T2	Create a visual comparison tool to determine if the prediction is current by comparing the prediction against the data at the same coordinate the next day. Pass: The error of the comparison is within 10%.				
U2	F3	S3	T3	Make a prediction using the chosen neural network model. Compare the prediction with the other trained models' estimations at the same location. Pass: The chosen model has the highest accuracy and closest to the desired accuracy of 90%.				
	F4	S4	T4	Compare the predictions where there was a previous discontinuity/break. Pass: The new model prediction does not contain the discontinuity/break and has an improved accuracy of more than 5%.				
U3	F5	S5	T5	Make an estimation of an ice chart in two locations, one in the Arctic and the other in the Antarctic. Pass: Both predictions are within the same accuracy.				
	F6	S6	T6	Predict ice charts in the Southern hemisphere. Pass: The predictions present no signs of overfitting.				
U4	F7	S7	T7	Make a prediction using the chosen neural network model. Pass: The input dimension is equal to the output dimension.				
	F8	S8	T8	Create a tool that classifies the variation of each image and assigns it with a resampled image variation. Apply the algorithmic tool to a data set. Pass: The images in the data set result in a variation greater than 0.05.				

Table 3.4: Table representing Acceptance Tests Protocol

3.4. ACCEPTANCE TESTS PROTOCOL

A list of Acceptance Tests in Table 3.4 were developed to ensure that the User Requirements are met by assessing the specification branches linking each requirement. Therefore, determining the success of the investigation.

A series of tests need to be conducted for each specification in Table 3.3 and assessed at the end of the investigation by analysing the final results. A pass requirement is provided for each test and overrides the replicability of each experiment. Meaning that none of the tests could be passed by chance and would have to produce definitive results that progressive the research in this field. At the end of the investigation, the tests are performed and deemed either pass or fail. Depending on the importance of each specification, it is necessary for the main tests to pass. Majority of the tests are passed inherently during the process of the investigation. However, certain tests require producing quantifiable results that directly correlate to the performance of the experiment. Performance in these tests is crucial in assessing what is achieved at the end of the investigation.

Chapter 4

Data Sources

The data sources presented in the Literature Review need to be analysed and assessed to determine if these sources are applicable for the specific implementation of estimating SIC's using Neural Networks. The selected data source needs to provide consistently accurate image data with high spatio-temporal resolutions.

4.1 Data Source Selection

For the purpose of this investigation, two data sources have to be selected, one source providing the input satellite images for the Neural Network model to train and the other source providing the output SIC images.

4.1.1 Satellite Image Data

Firstly, the selection of the input image source needs to be selected. Copernicus Open Access HUB is the only source analysed in the Literature Review that provides this specific data. The reason for this is because Copernicus sources the satellite images from the various SENTINEL missions, and if an alternative access hub were to be implemented, it would still provide the same SENTINEL data. Therefore, due to this source being implemented and tested in similar research [3][8], it was chosen to be carried through the conduction of this investigation.

The SENTINEL-1 satellite provides remote-sensed (SAR) images that best fit the high spatio-temporal resolution required for this investigation. The Copernicus online search interface allows the user to fine-tune the query when obtaining images retrieved from the satellite. This search can be applied to a specific area on the map based on a geographical polygon, which allows an area to be focused when obtaining images from the satellite and provides a suitable feature for a SIC estimation model.

4.1.2 Ground Truth Image Data

The second source is required to provide SIC images for both the Northern and Southern hemisphere. In analysing the data sources elaborated the literature review, one particular source stands out. The OSI-401-b product presents a promising tool for this investigation due to the inclusion of an uncertainty layer in each SIC label. This uncertainty layer can be incorporated into a loss function and implemented in a SIC estimation model. This product provides PMW sourced SIC images with superior spatio-temporal resolution compared to the products dispensed by the NSIDC. As seen in previous research [7], NSIDC data is more suited to Machine Learning models that are calibrated for monthly data. As this investigation focuses on producing SIC estimations with a high temporal resolution, the NSIDC data sources were disregarded.

4.2 Data Acquisition

Google Colab was used to download and pre-process the data from both of the selected sources onto a mounted Google drive. Colab is commonly used in Machine Learning implementations due to its accessibility to free cloud-based GPU's and data versatility. It also contains pre-installed libraries that will be utilised in this investigation, such as: *TensorFlow*, *keras*, *OpenCV*, *numpy* & *pandas*. The data acquisition method implemented here follows the same principle in a previous paper [3].

4.2.1 Copernicus SAR Images

Copernicus presents images based on the search criteria given to the search engine. The data found is relatively large when inspecting the satellite SAR image, this poses a problem as it is not suitable when automating a data acquisition algorithm for thousands

of images. It's impractical and time costly to download large images of one gigabyte in such large quantities. However, each image when searched provides a Quicklook image to preview the selection. This image is significantly smaller in size and can easily be downloaded using an automation algorithm in Colab.

The *sentinelsat* library was installed on Colab and assists in searching for the SENTINEL-1 images on Copernicus by presenting a command-line interface and powerful Python API. The *query* function in this library allows the user to specify the search requirements and region of interest for the downloaded images. These specifications are mentioned in the Literature Review and one of the advantages of this data source.

After all the images are found, they then have to be downloaded. The Python *Requests* library provides a tool that is able to download an image from an input URL. This is effective in this investigation as it can be paired with the search query results provided by Copernicus.

4.2.2 OSI-401-b SIC Images

The OSI-401-b product is distributed on various FTP server mirrors. CMEMS provides one such mirror and is able to be implemented. The *ftplib* Python library was used to download all the SIC files within the specified date range and store these file on the mounted Google drive. These files contained two labels, a SIC label and uncertainty label.

4.3 Data Pre-processing

The SAR images acquired from Copernicus often were downloaded having various dimensions. The images were all resampled to the same image dimension as per the input requirement for the Neural Network implementation.

Once all the Copernicus and OSI-401-b images were downloaded and resampled, they had to be labelled according to the corresponding coordinate of each SAR image. An *OData* footprint contained in each downloaded SAR image presents the latitude and longitude coordinate locations of the corners within each image.

To pair each corresponding concentration label to the SAR image, a pixel coordinate system was created based on image footprint. To match this footprint in the concentration label, a smaller patch within the concentration label was extracted that was made to mirror the corresponding SAR image. This can be seen in Figure 4.1 below where the same process was performed on the uncertainty label.

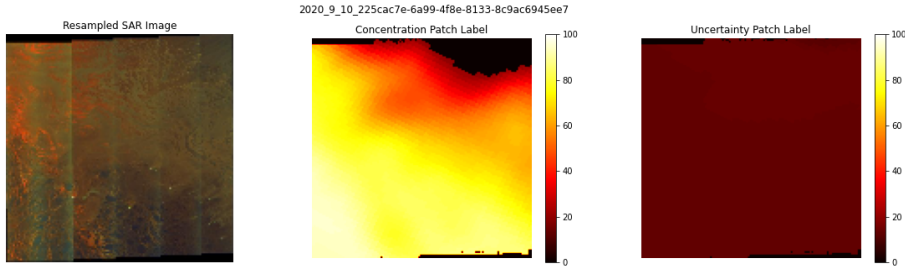


Figure 4.1: The resampled SAR image presented with its corresponding SIC and uncertainty label.

4.4 Data Curation

In order to prevent the Neural Network models from learning unimportant data, a selection process was developed that curated all the images within each data set. It is important for the Neural Network model to pass through images containing useful data. This means that images used as inputs to the model should contain variation in SIC. An image that displays 100% or 0% SIC presents no room for improvement in SIC estimation models. Therefore, a selection process is needed to filter out the unimportant images.

A data curation algorithm was created that disregards all SAR images producing a variance below the minimum threshold of 0.05 along with its corresponding OSI-401-b labels. This can be seen below in Figure 4.2 where the SAR image is selected for the next stage of the investigation as its variance satisfies the minimum threshold.

4.4. DATA CURATION

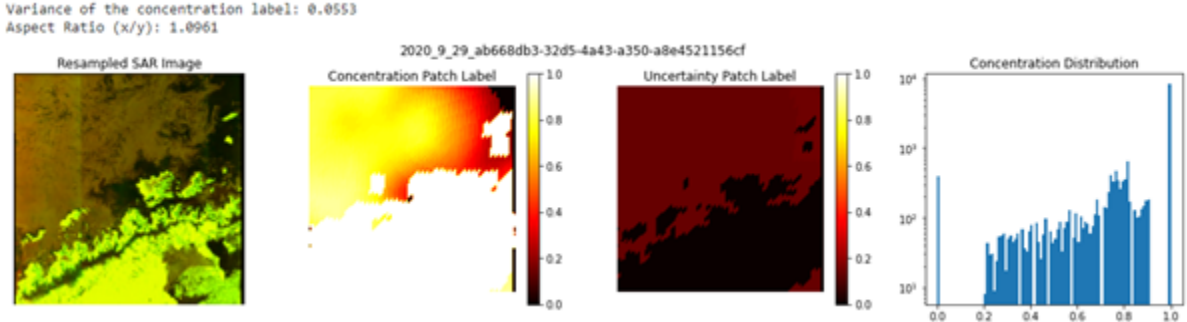


Figure 4.2: This SAR image is selected in the data curation process as it contains a variation of 0.0553 which is above the minimum threshold of 0.05. It Also displays a histogram of the concentration distribution within the SAR image.

The same cannot be observed in Figure 4.3 as its variance is below the minimum threshold and presents no use for the Neural Network implementation stage.

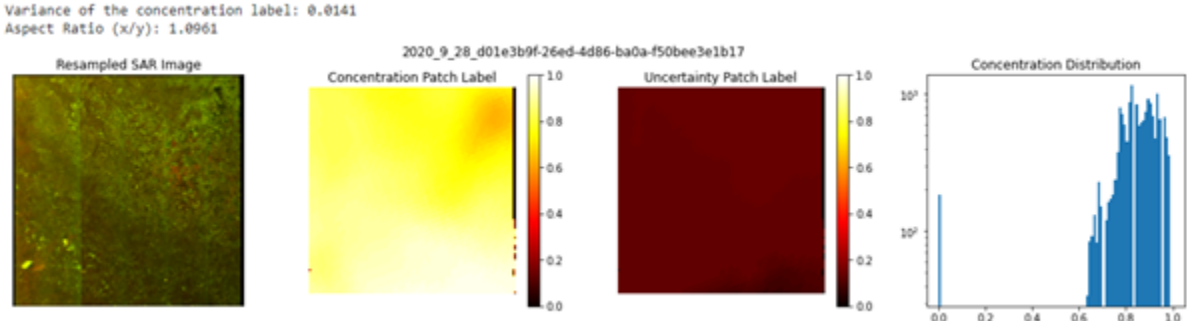


Figure 4.3: This SAR image is disregarded in the data curation process as it contains a variation of 0.0414 which is below the minimum threshold of 0.05. It Also displays a histogram of the concentration distribution within the SAR image.

In performing the data curation process, a large number of images are disregarded. This reduces the size of each data set and negatively affects the already minimal amounts of data in the Southern hemisphere. A summary of these data sets can be viewed in Table 4.1 detailing the regions implemented in the next stage.

4.5 Summary of Data Sets

A summary of all the data sets obtained in the data acquisition process is presented in Table 4.1. A dedicated focus based on the information regarding seasonal cycles in both the Northern and Southern hemisphere was implemented with the goal in determining if this additional information improved the results of SIC estimations using Machine Learning while introducing new alternative models.

Summary of Data Sets					
Data Set	Period of Acquisition	ROI	Seasonal Cycle	Total Images	Curated Images
Southern_Freezing	01/04/2020 - 30/09/2020 (6 Months)	Antarctic	Freezing	4881	655 (13.42%)
Southern_Melting	01/01/2020 - 30/06/2020 (6 Months)	Antarctic	Melting	5293	1867 (35.27%)
Northern_Freezing	01/01/2020 - 30/06/2020 (6 Months)	Arctic	Freezing	21285	3728 (17.51%)
Northern_Melting	01/08/2020 - 30/10/2020 (3 Months)	Arctic	Melting	11071	5286 (47.74%)

Table 4.1: Table representing a summary of the data sets used to train the models

Two data sets for each region was acquired, one during the freezing period and the second during the melting period. This was done to analyse the effects of implementing seasonal cycles in Neural Networks. All the data sets were acquired for a period of six months except the Northern hemisphere during its melting period. this is due to the need for the most recent available to be implemented for the Neural Network providing a high temporal resolution. In spite of the acquisition being halved compared to the other data sets, it in fact provided the models with the most "useful" data as seen in the Curated Images column, even more than the Northern freezing data. This trend of more curated images present in the respective melting periods is due to there being likely more coastlines and sparse patches of ice (floes). These types of sea ice gives rise to higher amounts of data containing variance than the sea ice during the freezing period.

4.6 Analysing Errors in Data Sources

Certain errors in the data sources were found during the investigations conducted in previous research [3]. This error pertained to the orientation of the SAR images obtained from Copernicus Open Access HUB. This error will be inspected in the images and a resolution will be found if the error persists.

4.6.1 Pass Direction Mislabelling

It appeared in past research that the satellite orbit when remote-sensing the images moves in an oscillatory trajectory from East to West. When the satellite travels from the South to the North it performs its ASCENDING pass, and when the satellite travels from the North to the South it performs its DESCENDING pass. Evidence in mislabeling of images obtained in the ASCENDING pass occurred as the images appeared to be rotated by 180° as seen in Figure 4.4.

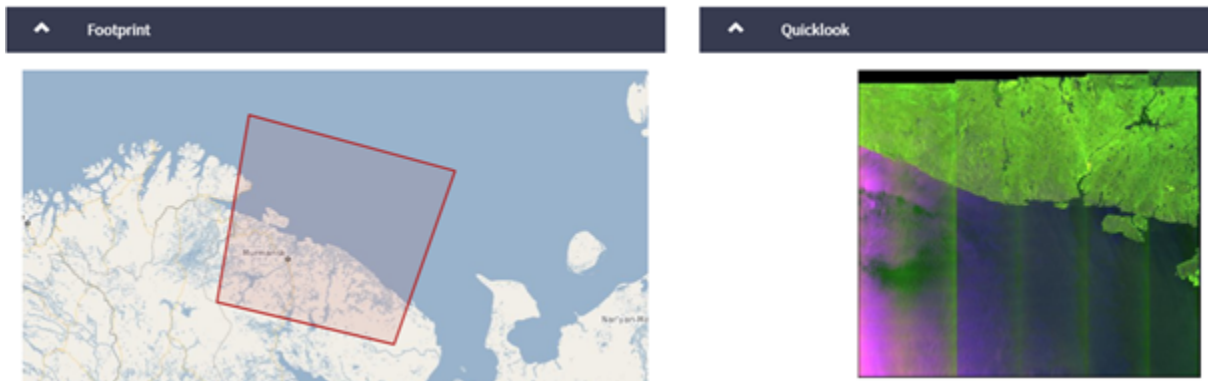


Figure 4.4: This SAR image was obtained during the satellites ASCENDING pass and displays the correct image footprint as well as the rotation error.

In Figure 4.5 below, the satellite path is mapped for an ingestion period during October 2020. It is clear that the error still exists due to the only ASCENDING pass images being highlighted in bright red. The other images are clearly obtained in the DESCENDING pass identified by the East to West trajectory travelling from North to South. However, these DESCENDING images are pre-processed correctly and matches its the footprint.



Figure 4.5: A series of images retrieved from the satellite mapping the satellites trajectory of ingestion.

4.6.2 Error Correction

A solution found in [3] was found in 2019 as this error still existed at the time. The same solution is implemented in this investigation and involves using the latitude and longitude coordinates of the four corners of the *OData* footprint to detect in which pass direction the SAR images were obtained. If the calculated pass direction matched pre=processed pass direction, the image orientation is correct. if not then the image is flipped by 180° to make the correction.

This process was performed before the image resampling stage and allowed the data to be correctly prepared for Neural Network implementation.

Chapter 5

Neural Networks

When looking at newer or alternative architectures it is apparent that it would need to be adapted for the specific application of SIC estimation. Based on the information presented in the literature review, models that implemented a simple downsample-upsample architecture performed the best and provided higher accuracy.

Two different Neural Networks were implemented during the conduction of this investigation. The first being a simple AutoEncoder network architecture essentially acting as a control network that presents results for comparisons. The second network to be implemented is a LinkNet Neural Network, this model will be the main focus during the conduction of this investigation and will be compared to the results of previous models.

5.1 Convolutional AutoEncoder Network

The AutoEncoder network architecture is trained in an unsupervised manner and also presents an unexplored alternative for estimating SIC's. The model created with this architecture takes in a SIC image as an input and attempts to recognise patterns within the image and reconstruct these learned patterns to produce a model prediction.

There are specific advantages when training using an AutoEncoder architecture presented in Figure 5.1 below.

Some stand out advantages are presented here which pleads the case for the use of AutoEncoders in SIC estimation efforts:

1. Provides multiple filters that can best fit the given data.
2. Tends to improve data performance, but this is not always the case and can sometimes reduce data performance
3. Produces a model based on input data rather than providing a predefined filter.

This investigation aims to make use of these advantages and provide an adequate SIC estimation model capable of contributing to the gap in Southern hemisphere research.

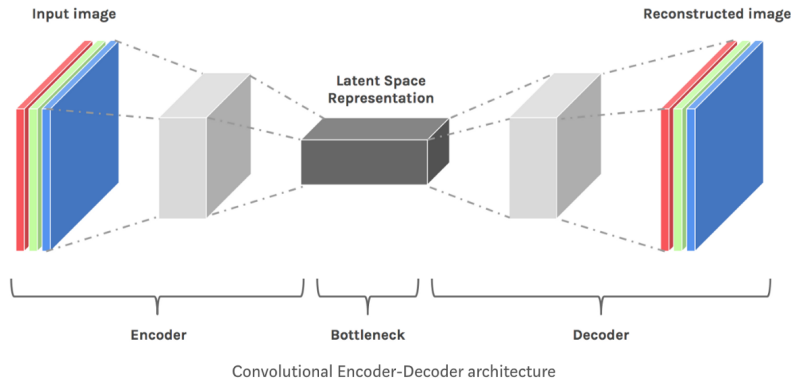


Figure 5.1: A diagram illustrating the connections within the AutoEncoder architecture.

5.1.1 Implementing the AutoEncoder for SIC Estimations

Due to the nature of the AutoEncoder network, it is not necessary to make any drastic changes to the network itself. The network uses "same" padding on all the applicable functions with a sigmoid activation layer at the output layer. This model produces a SIC estimation with the same output image dimension as the input.

For the code, a model definition implementing *keras* was found on a GitHub repository [9] and used for the majority of the convolutional AutoEncoder architecture creation.

5.2 LinkNet

LinkNet is an advanced supervised Neural Network based on a simple encoder-decoder architecture which is represented in Fig. 5.2 below. It is commonly implemented for use in pixel-wise semantic segmentation algorithms due to its ability to process high

resolution images. The reason it is chosen over other neural networks is because of its efficiency and timeliness while utilising all the parameters within the network. The number of parameters is considerably less compared to similar network architectures like UNet, with the number of parameters approximately close to 120 million [3]. This amount of parameters is significantly larger than the LinkNet architecture, which has an approximate number of 11 million parameters [10]. This parameter reduction, close to a factor of 10, speeds up the training process of the model compared to other similar network architectures implemented in the past.

Another benefit of LinkNet is the use of *skip connections*. Skip connections help traverse information in deep neural networks. Gradient information can be lost as we pass through many layers, this is called vanishing gradient. Advantages of skip connection are they pass feature information to lower layers so using it to classify minute details becomes easier. As MaxPooling is performed some amount of spatial information is lost. Skip connections can help increasing the classification accuracy because the final layer feature will have more information.

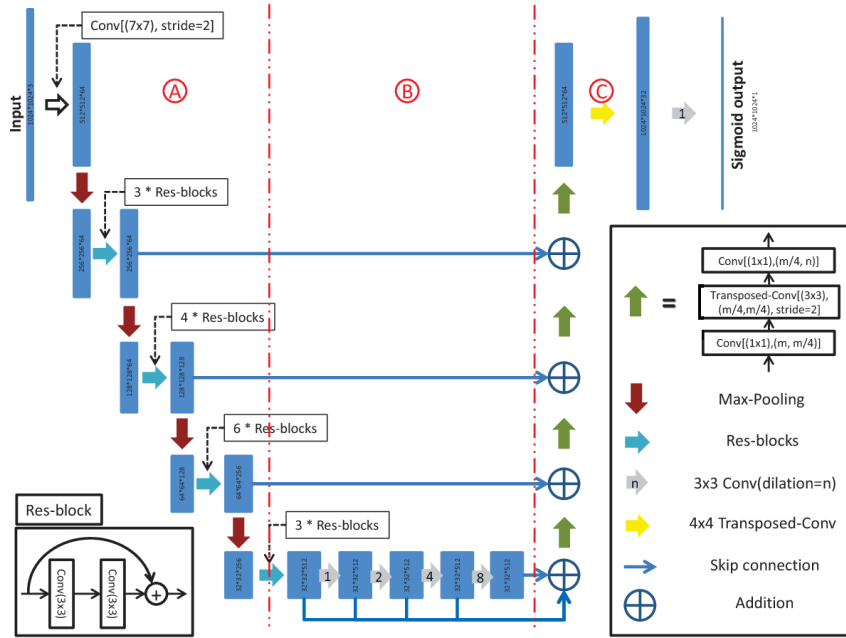


Figure 5.2: A diagram illustrating the connections within the LinkNet architecture.
Source: Adapted from [11].

Although LinkNet is a variation of the previously implemented UNet, it does contain specific features that separate the network architectures from one another in the following manner [12]:

1. UNet's ordinary convolution structure is replaced with a residual module (Res-

Blocks).

2. UNet’s deep and shallow feature synthesis method is transformed from concatenating (“stacking”) to adding.

The differences and improvements mentioned above compared to previous network architectures provides a promising potential for the implementation of a SIC estimation model.

5.2.1 Implementing LinkNet for SIC Estimations

The LinkNet architecture in its original form cannot immediately be implemented for SIC estimations since it was originally intended for image segmentation. Therefore, the inner architecture needs to be adapted while still maintaining the core features of the original architecture.

An implementation of the LinkNet architecture found on GitHub using the *Keras* library [13]. This code was used for the bulk of the model definition during the neural network implementation.

By acquiring the code from the GitHub repository it was then ready to be adapted to produce SIC estimations. The single adaptation in the original architecture was to change the padding of each convolutional and MaxPooling layer from “valid” to “same” where applicable. This change in the padding parameter for each function ensured that the output image dimension would be identical to the input image dimension and passes T7 in Table 3.4.

Chapter 6

Model Training and Evaluation

The models presented throughout this investigation were trained with varying input features regarding the following parameters:

- Model Type : AutoEncoder/LinkNet
- Training Region: Arctic (N)/Antarctic (S)
- Training Region Cycle: Freezing (F)/Melting (M)
- Testing Region: Arctic (N)/Antarctic (S)
- Testing Region Cycle: Freezing (F)/Melting (M)

6.1 Model Naming Convention

Because of the complex process when training each Neural Network model, it is essential to develop a model naming convention, in order to keep track of the features used for each model trained.

There are two different naming conventions implemented throughout the model training process of the investigation. Firstly, while training the models, if the training data and testing data were both acquired during the same seasonal cycle (freezing/melting), then the model would be named according to the following labelling structure:

ModelType_TrainingRegion_TestingRegion_SeasonalCycle

For example, **LinkNet_S_S_M**, would refer to the model being trained with the **LinkNet** architecture, trained on Southern (**S**) data, tested on Southern (**S**) data and both these training and testing data were acquired during the melting period (**M**) in the Antarctic.

The second naming convention was used on models that were trained and tested on during different seasonal cycles. These models were named according to the following labelling structure:

ModelType_TrainingRegionSeasonalCycle_TestingRegionSeasonalCycle

An example of this would be the **LinkNet_NF_SM**, this label indicates that the model is trained using the LinkNet architecture, trained on Northern data acquired during the freezing period (**NF**) and tested on Southern data acquired during the melting period (**SM**).

6.2 Model Training Process

The models were defined using a *Functional API* approach provided by the *keras* library. This elected method allows the models to learn deep patterns as well as simple rules within the images presented. The training of each model was initiated by the `model.fit()` function, where a summary of the inner layers was displayed as well as the loss metrics being documented throughout the training and evaluation of the model.

Each standard model was trained for 50 epochs using the aforementioned function. Nonstandard models, models trained with transfer learning, were trained with one set of data for 32 epochs during the first stage of the training process, then the second stage of training was performed for 18 epochs on the second set of data. This totalled to an amount of 50 epochs for the transfer learning approach.

The loss function which was chosen to be implemented undergone a trial and error process which allowed the model to produce effective results with regards to accuracy and performance. Each loss function separates the uncertainty label and concentration label from the ground truth image which is then used to perform a pixel-wise error analysis on the predicted SIC image.

6.2. MODEL TRAINING PROCESS

Based on previous research conducted with UNet [3], a loss function was applied that involved weighting the mean absolute error (MAE) loss values with the uncertainty layer (obtained from OSI-401-b product). This application of weighting the standard MAE loss function allowed the model to focus on specific areas of the SIC images where minimal estimation error occurs.

This loss function was compared to other loss functions of varying definitions presented below and the summary of the results can be viewed in Table 7.1 & 7.2:

- Mean Absolute Error (MAE)
- Uncertainty Weighted Mean Absolute Error (UW MAE)
- Uncertainty Biased Mean Absolute Error (UB MAE)
- Mean Square Error (MSE)
- Uncertainty Weighted Mean Square Error (UW MSE)
- Uncertainty Biased Mean Square Error (UB MSE)

As listed above, an uncertainty biased loss was defined that prioritises pixels in the SIC image based on the "certainty" layer (created by inverting the values of the uncertainty layer).

At the close of the trial and error process, the loss function that provided the best results for each section was used to train the final model for the respective regions and seasonal cycles.

Chapter 7

Results

The models obtained throughout the training process were all created with the objective of producing SIC estimations in the Southern hemisphere. Various models where trained containing specific features that produced beneficial results regarding the investigation.

7.1 Model Performance

An analysis of the LinkNet model losses is presented below. The choice in the omission of the AutoEncoder model losses will be explained in the next section as it is not needed at this stage.

The top two sections in which Table 7.1 & 7.2 are divided contains information of the losses regarding the Southern hemisphere during its specific seasonal cycle. With the first section representing the freezing period, and the second section representing the melting period. The last section of each table contains results based on testing in the Northern hemisphere. This section was used as a comparison to the Southern hemisphere models.

7.1.1 Mean Absolute Error Losses

In Table 7.1 the MAE loss and its variations are presented for each LinkNet model, these losses are separated to highlight the seasonal cycle for which the model was tested on.

Model	UW MAE		UB MAE		MAE	
	Train	Test	Train	Test	Train	Test
LinkNet_S_S_F	0.1649	0.1832	0.0301	0.0466	0.0815	0.1021
LinkNet_NS_S_F	0.2262	0.2580	0.0328	0.0640	0.0846	0.1218
LinkNet_SM_SF	0.1286	0.1371	0.0403	0.0452	0.0959	0.1057
LinkNet_NM_SF	0.0489	0.1652	0.0222	0.1061	0.0410	0.1739
LinkNet_NF_SF	0.0585	0.1554	0.0157	0.0882	0.0408	0.1518
LinkNet_S_S_M	0.0962	0.1291	0.0218	0.0499	0.0572	0.0954
LinkNet_NS_S_M	0.1711	0.2110	0.0458	0.0856	0.0911	0.1383
LinkNet_SF_SM	0.2210	0.2231	0.0887	0.1336	0.1433	0.1455
LinkNet_NM_SM	0.0489	0.1744	0.0222	0.1284	0.0410	0.1832
LinkNet_NF_SM	0.0585	0.1742	0.0157	0.1170	0.0408	0.1725
LinkNet_N_N_F	0.0585	0.0925	0.0157	0.0420	0.0408	0.0802
LinkNet_N_N_M	0.0489	0.0720	0.0222	0.0404	0.0410	0.0672

Table 7.1: A summary of the Mean Absolute Error of each model during the training and testing phase. The losses highlighted in green represent the best testing loss for that specific loss variant of its respective section (freezing/melting). The losses highlighted in blue represent the best overall testing loss for each section (freezing/melting)

In analysing the table above, the following key observations standout:

The uncertainty biased MAE loss is the lowest out of all the losses during the training and testing phase of each model.

It appears that models trained during the melting period in the Southern hemisphere have the highest performance compared to other training data. This is apparent in two instances when comparing the testing loss for each model. In the first instance, we focus on the models in the first section (tested on freezing Southern hemisphere images), when comparing LinkNet_S_S_F and LinkNet_SM_SF, the testing loss for LinkNet_SM_SF is less than for LinkNet_S_S_F except in the case of the pure MAE loss. Note that the UB MAE and MAE losses for both of these models are quite close in comparison, hence the outlying loss highlighted in green for the MAE results. The same cannot be said for the UW MAE losses, where the difference margin is significantly larger with the LinkNet_SM_SF loss providing a better performance and the second nearest loss is provided by the LinkNet_NF_SF model. A plausible conclusion in favour of the melting data over the freezing data can be made that due to the UW MAE testing loss performing notably

7.1. MODEL PERFORMANCE

better even though the other two losses are relatively close respectively.

The second instance compares the models in the Southern melting section of the table. All the testing loss variants in the LinkNet_S_S_M are superior to the other models with the UB MAE loss providing the best performance (highlighted in blue). The closest model to provide comparison is the LinkNet_NF_SM model. This could be attributed to the similar marginal ice zone present during the specific seasonal cycle for each region. Meaning that the data during the melting period in the South share some similarities with the data acquired during the freezing period in the North.

These losses (LinkNet_SM_SF & LinkNet_S_S_M) were compared to the losses produced in the next stage of the results.

An important note to make that in the last section, the models trained and tested in the North all performed better than the models tested on the Southern images. This is notable because the increase in performance is likely due to the large amount of training data images in the North provided to the LinkNet model, as seen in Table 4.1.

7.1.2 Mean Square Error Losses

Table 7.2 below follows the same structure as Table 7.1, it documents the MSE losses and its variants for the LinkNet models.

Model	UW MSE		UB MSE		MSE	
	Train	Test	Train	Test	Train	Test
LinkNet_SS_F	0.0181	0.0261	0.0124	0.0182	0.0221	0.0324
LinkNet_NS_SS_F	0.0158	0.0313	0.0095	0.0215	0.0190	0.0390
LinkNet_SM_SF	0.0226	0.0201	0.0123	0.0111	0.0290	0.0257
LinkNet_NM_SF	0.0123	0.0591	0.0099	0.0433	0.0158	0.0759
LinkNet_NF_SF	0.0085	0.0518	0.0058	0.0383	0.0106	0.0660
LinkNet_SS_M	0.0106	0.0242	0.0071	0.0161	0.0128	0.0303
LinkNet_NS_SS_M	0.0232	0.0461	0.0168	0.0355	0.0280	0.0581
LinkNet_SF_SM	0.0480	0.0505	0.0887	0.0922	0.0594	0.0625
LinkNet_NM_SM	0.0123	0.0783	0.0099	0.0652	0.0158	0.0999
LinkNet_NF_SM	0.0085	0.0718	0.0058	0.0587	0.0106	0.0915
LinkNet_N_N_F	0.0085	0.0239	0.0058	0.0173	0.0106	0.0306
LinkNet_N_N_M	0.0123	0.0217	0.0099	0.0169	0.0158	0.0279

Table 7.2: A summary of the Mean Square Error of each model during the training and testing phase. The losses highlighted in green represent the best testing loss for that specific loss variant of its respective section (freezing/melting). The losses highlighted in blue represent the best overall testing loss for each section (freezing/melting)

The MSE losses provided better overall performance than the MAE losses in Table 7.1 and presented more consistent results. This is observed in both sections of the table (South freezing and melting) where the models trained on the Southern melting data provided the best results.

Unlike the MAE losses, the difference margins for each model loss is consistent, with the closest models being the LinkNet_SS_F & LinkNet_NS_SS_M for the Southern Freezing & melting data respectively.

Another difference in comparing the tables is noted regarding the models trained with transfer learning. These models were first trained on Northern data for a certain amount of epochs and completed training utilising the Southern data. The performance of these models is greatly improved compared to the MAE models, where these models performed

the worst. Although these models performed as required, the models trained with the Southern melting data provided the best results, which is the same result in the MAE models.

The LinkNet_SM_SF & LinkNet_S_S_M were the models that indicated the best performance and continued to be implemented throughout the investigation. These were not the final models as the model predictions need to be visually analysed due to the nature of the losses being weighted/biased.

7.2 Comparing Model Predictions

7.2.1 Convolutional AutoEncoder vs. LinkNet

As mentioned in the model performances section, the losses for the AutoEncoder models were not presented for analysis. The reason for this omission is elaborated below. One of the inherent requirements of the models is that the predicted SIC estimations have to visually resemble the ground truth image. This pertains to image dimensionality, colour, distinguishing small land masses and presenting a SIC estimation relevant to the concentration key paired with each SIC.

In Figure 7.1 & 7.2 below, we analyse the predictions in the Southern hemisphere made by models created using a LinkNet and AutoEncoder architecture. These models each produced a prediction provided with the same SAR image as the input.

In Figure 7.1, the LinkNet model produces a SIC image that resembles the ground truth image in terms of image dimension and colour. It is also able to distinguish small landmasses as demonstrated with the small concentration patch highlighted in the bottom right of the ground truth image which can be seen in the model prediction. The prediction distinguishes specific land masses (red/yellow) from the sea (black) without any blending of colour. This separation is directly correlated to the colour key on the right representing the SIC level.

7.2. COMPARING MODEL PREDICTIONS

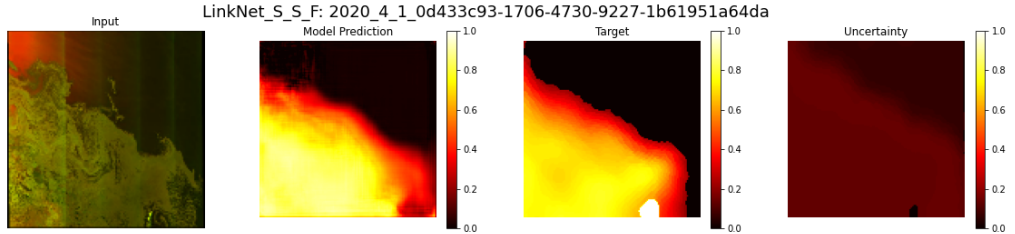


Figure 7.1: A LinkNet model trained and tested on Southern hemisphere data during its freezing period. The figure contains 4 images, the input to the model, the prediction produces by the model, the ground truth image for which the prediction is compared to and the uncertainty label obtained from the OSI-410-b product.

The same cannot be said for the AutoEncoder model prediction. Although the image dimension is equal, and it is able to separate the land mass from the sea, it fails in representing this information in terms of colour. This prediction error can be identified due to the sea being estimated to a reddish colour. This is incorrect as there is no sea ice present in that location proven by the ground truth SIC. Another disability present in this model is the inability to recognise small concentration patches. As of now it seems the AutoEncoder is insufficient in providing a valid SIC estimation model, but a further analysis has to be undertaken.

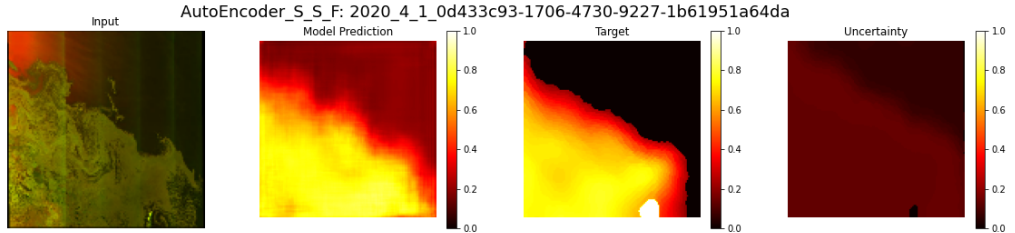


Figure 7.2: An AutoEncoder model trained and tested on Southern hemisphere data during its freezing period. The figure contains 4 images, the input to the model, the prediction produces by the model, the ground truth image for which the prediction is compared to and the uncertainty label obtained from the OSI-410-b product.

One theory for the cause of this red colour in the predictions is the minimal amount of image data in the Southern hemisphere. To test this, a SIC prediction on the same image was produced by models trained SIC images in the Northern hemisphere. These predictions are presented below in Figure 7.3 & 7.4, referring to the LinkNet and AutoEncoder

7.2. COMPARING MODEL PREDICTIONS

models respectively.

The LinkNet model meets all the requirements for a valid SIC estimation model. It is excellent in its ability to recognise small land masses located in the top left of the SIC ground truth image and prediction. It provides improved concentration accuracy in terms of colour when comparing it to both the predictions in the Southern hemisphere, even more so in the case of the AutoEncoder prediction.

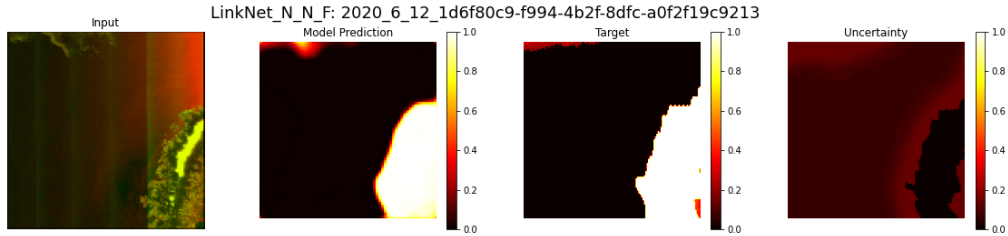


Figure 7.3: A LinkNet model trained and tested on Northern hemisphere data during its freezing period. The figure contains 4 images, the input to the model, the prediction produced by the model, the ground truth image for which the prediction is compared to and the uncertainty label obtained from the OSI-410-b product.

Comparing the AutoEncoder prediction below to the Southern hemisphere model, it can be observed that this model is an improvement. The reddish colour of the sea in the previous model is still visible but darker in colour. This model is also able to recognise small land masses (top left corner), unlike the Southern hemisphere AutoEncoder model. Although this model is an improvement, it is still not up to standard for application in the Southern hemisphere. The theory of training an AutoEncoder model with a larger data set proved correct with the improvements mentioned above, but there is not enough data at this time for use of this model to be effective.

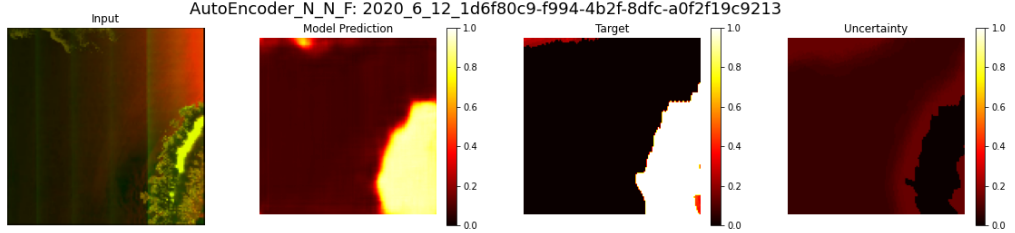


Figure 7.4: An AutoEncoder model trained and tested on Northern hemisphere data during its freezing period. The figure contains 4 images, the input to the model, the prediction produces by the model, the ground truth image for which the prediction is compared to and the uncertainty label obtained from the OSI-410-b product.

7.2.2 UW MAE vs. UB MSE

The UW MAE loss was chosen to be compared to the UB MSE loss, which is the best performing loss metric presented in Table 7.1 & 7.2. The SIC estimations produced by these models need to be visually analysed to meet the requirements.

The UW MAE model below meets all the visual requirements for it to be considered as a viable model. The concentration distribution is even and resembles the ground truth SIC image. The yellow concentration patches present in the inland sea ice tend more to an orange colour closer to the ground truth SIC image. This model poses a viable model for the investigation but needs to be compared to the UB MSE loss model.

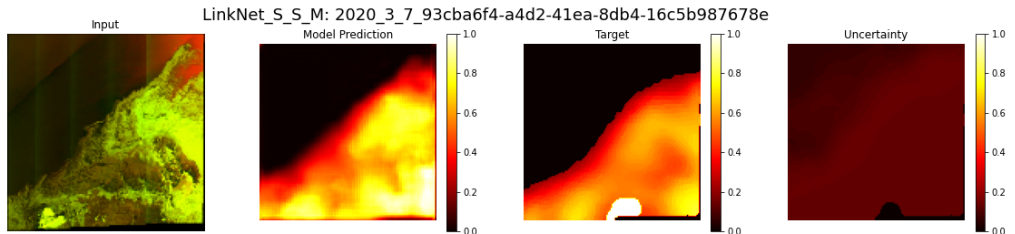


Figure 7.5: A LinkNet model trained and tested on Southern hemisphere data during its melting period using UW MAE as the loss. The figure contains 4 images, the input to the model, the prediction produces by the model, the ground truth image for which the prediction is compared to and the uncertainty label obtained from the OSI-410-b product.

7.2. COMPARING MODEL PREDICTIONS

In comparing the UW MAE model above with the UB MSE model below, two differences stand out. The yellow concentrations are much brighter than the ground truth image and display a hazy visual when mapping the SIC. The concentration is not evenly distributed, unlike the UW MAE model. These two points highlight the errors in the UB MSE model, proving the UW MAE model as the superior choice.

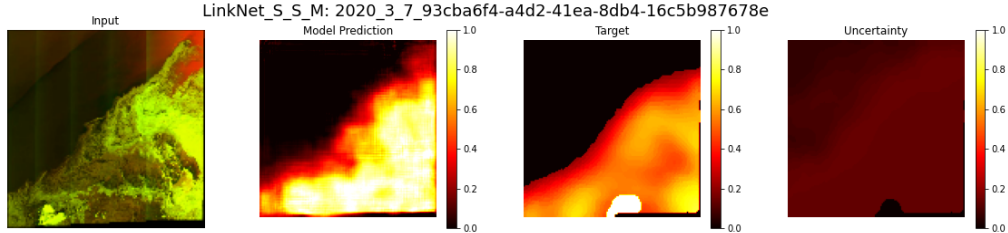


Figure 7.6: A LinkNet model trained and tested on Southern hemisphere data during its melting period using UB MSE as the loss. The figure contains 4 images, the input to the model, the prediction produces by the model, the ground truth image for which the prediction is compared to and the uncertainty label obtained from the OSI-410-b product.

7.2.3 Southern Hemisphere (Freezing)

The UW MAE loss was chosen to be implemented based on the visual analysis above and continued to be analysed for the conduction of the investigation.

The freezing period in the Southern hemisphere will be applied to two models, LinkNet_-SM_SF and LinkNet_NF_SF. These models were chosen based on the model performance assessment for each loss metric.

The LinkNet_SM_SF in Figure 7.5 below meets all requirements provided by the visual assessment criteria implemented previously and shows no signs of overfitting. There is a slight difference in the prediction ground truth SIC image, where the yellow is not as bright as needed to be, but this can be overlooked as it is a minor detail.

7.2. COMPARING MODEL PREDICTIONS

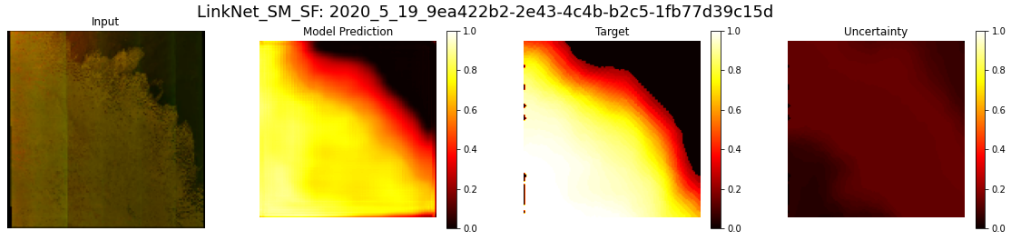


Figure 7.7: A LinkNet model trained on Southern hemisphere data during its melting period and tested on Southern hemisphere data during its freezing period. The figure contains 4 images, the input to the model, the prediction produces by the model, the ground truth image for which the prediction is compared to and the uncertainty label obtained from the OSI-410-b product.

The LinkNet_NF_SF model in Figure 7.8 below was trained in the North during its freezing period and tested in the South during its respective freezing period. The model prediction passes all the requirements of the visual assessment criteria except one. The prediction provides excellent ability to separate sea and ice and display concentrations with the correct colour brightness. But it fails in distinguishing the border of the SIC and incorrectly increases its size. This is likely a result of overfitting when training on the data in the Northern hemisphere. Another likely cause could be attributed to the geological differences present that affect both the Southern and Northern SIC's. Therefore, the LinkNet_SM_SF model is chosen as the final model to be implemented in the Southern hemisphere during its freezing period due to its superior ability in displaying the SIC estimations accurately.

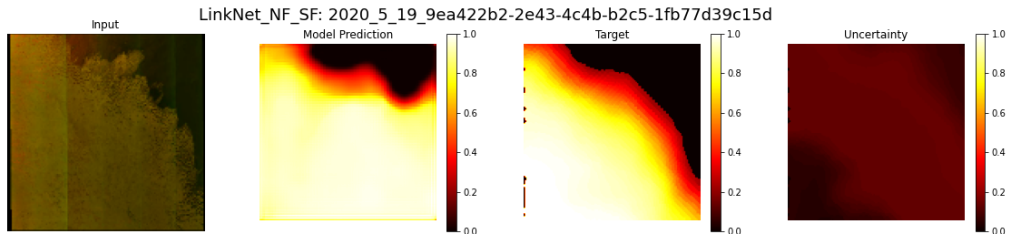


Figure 7.8: A LinkNet model trained on Northern hemisphere data during its freezing period and tested on Southern hemisphere data during its freezing period. The figure contains 4 images, the input to the model, the prediction produces by the model, the ground truth image for which the prediction is compared to and the uncertainty label obtained from the OSI-410-b product.

7.2.4 Southern Hemisphere (Melting)

For the melting period in the Southern hemisphere, the following models were chosen to be analysed, LinkNet_S_S_M and LinkNet_NF_SM. These models, like the freezing period models, were chosen during the model performance assessment process.

The LinkNet_S_S_M model below produces accurate SIC estimations with an even distribution of the colour representing the SIC's. The colour is not overly bright and shows no signs of overfitting. Although the edges are hazy in some areas, the model still provides an effective model to be implemented in the Southern hemisphere.

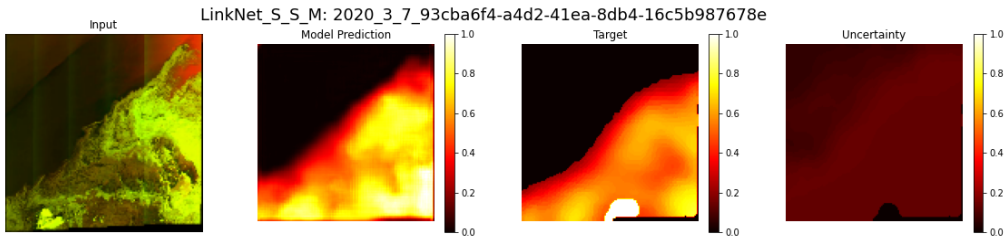


Figure 7.9: A LinkNet model trained and tested on Southern hemisphere data during its melting period using UW MAE as the loss. The figure contains 4 images, the input to the model, the prediction produced by the model, the ground truth image for which the prediction is compared to and the uncertainty label obtained from the OSI-410-b product.

Comparing the LinkNet_NF_SM model below to the model above presents a stark contrast in the SIC predictions produced by each model. The model below is trained on Northern freezing data and produces an excessively bright SIC prediction with almost 100% concentration. This prediction is certainly incorrect as seen in the ground truth image. Therefore, it is obvious that the LinkNet_S_S_M model is more accurate as it presents its predictions in a manner that visually resembles the ground truth SIC image effectively.

7.3. CORRECTING DISCONTINUITIES WITHIN THE PREDICTIONS

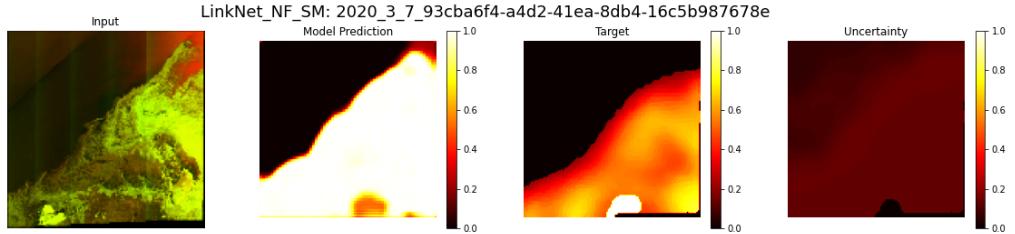


Figure 7.10: A LinkNet model trained on Northern hemisphere data during its freezing period and tested on Southern hemisphere data during its melting period. The figure contains 4 images, the input to the model, the prediction produces by the model, the ground truth image for which the prediction is compared to and the uncertainty label obtained from the OSI-410-b product.

7.3 Correcting Discontinuities within the Predictions

One of the specifications mentioned in Table 3.3, explains the need for implementing external information to correct discontinuities/breaks in the SIC predictions made by each model. The models were created using data acquired during a specific seasonal cycle. This information was used to fine-tune each model and give it the ability to produce improved and accurate models.

In Figure 7.11 below, a SIC estimation was produced by a model trained with Southern freezing data. This particular prediction was chosen to illustrate the discontinuities within the predictions for this model. A large black hole can be observed in the model prediction that is clearly incorrect when comparing it to the relative ground truth image. This could likely be caused by the minimal data present in the southern hemisphere during its freezing period.

7.3. CORRECTING DISCONTINUITIES WITHIN THE PREDICTIONS

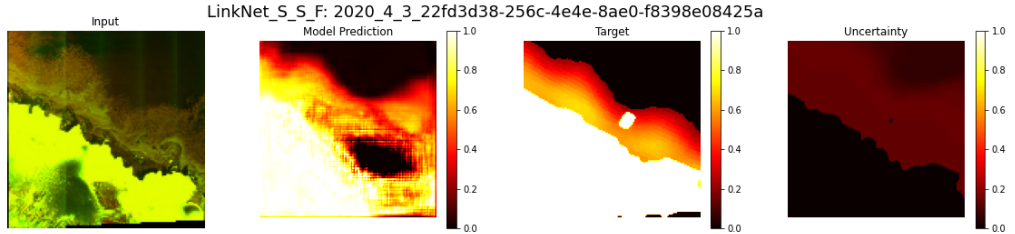


Figure 7.11: A LinkNet model trained and tested on Southern hemisphere data during its freezing period. The figure contains 4 images, the input to the model, the prediction produces by the model, the ground truth image for which the prediction is compared to and the uncertainty label obtained from the OSI-410-b product.

As it is a requirement for this investigation that the chosen model has the ability to correct discontinuities, a solution was sought to be found. For the sake of the investigation, the same SAR image in Figure 7.12 is used in Figure 7.12 to make a prediction. As the discontinuity presented itself when testing on Southern freezing data, the LinkNet_SM_SF model was chosen, as it presented the best results for this region of data.

Analysing the LinkNet_SM_SF model prediction below, an immediate improvement can be seen. The discontinuity which was previously an issue has now almost completely disappeared. This result satisfies the specification in Table 3.3 and passes T4 in Table 3.4.

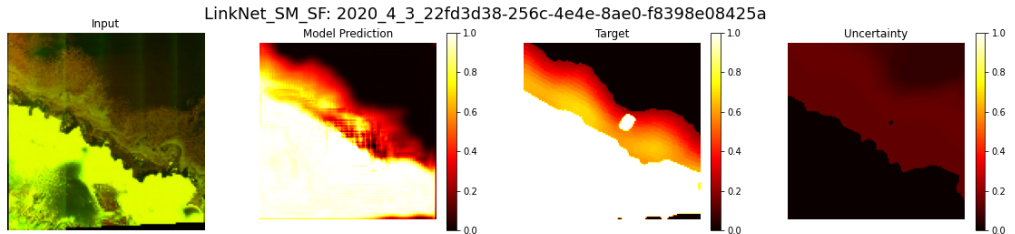


Figure 7.12: A LinkNet model trained on Southern hemisphere data during its melting period and tested on Southern hemisphere data during its freezing period. The figure contains 4 images, the input to the model, the prediction produces by the model, the ground truth image for which the prediction is compared to and the uncertainty label obtained from the OSI-410-b product.

7.4 Acceptance Tests

After the conduction of the investigation occurred, an analysis of the Acceptance Tests derived at the beginning was undergone. These tests were created to ensure progressive results that benefit the field in which this investigation falls under.

Acceptance Tests Outcome	
ID	Pass/Fail
T1	Pass: It can be observed in all the predictions comparing it against the ground truth SIC. One example being in Figure 7.3 where the land mass position in the image is identical.
T2	Fail: The loss for both models implemented for the Southern hemisphere during its respective freezing and melting period were both higher than 10%. LinkNet_SM_SF - 13.71% LinkNet_S_S_M - 12.91%
T3	Pass: The final chosen models presented the highest accuracy and reasonably close to 90%.
T4	Pass: The discontinuity within the prediction in Figure 7.11 was corrected in Figure 7.12 due to the model for second prediction having more Southern training data.
T5	Fail: The predictions made in the North performed significantly better than the predictions in the South. The results of transfer learning did not satisfy the loss requirements by any means.
T6	Pass: The final models for each seasonal cycle produced predictions that present no signs of overfitting. However, models trained in the North and tested in the South show signs but was not chosen.
T7	Pass: Due to the nature of the LinkNet architecture, the input and output image dimensions are equal.
T8	Pass: Only the SAR images with a variation greater than 0.05 was chosen in the Data Curation process.

Table 7.3: The outcomes of the Acceptance Tests derived at the beginning of the investigation

The acceptance tests were performed and produced the following results. Six out of the eight tests passed and two failed. T2 failed because the loss was higher than the required maximum of 10%, this could have been avoided by choosing an alternative loss metric as seen in Table 7.1 & 7.2, but implementing a model with a different loss gave rise to visual

7.4. ACCEPTANCE TESTS

issues in term of model predictions. Thus the final models chosen to be implemented are acceptable within reason. The second test to fail is T5, the Northern trained models all produced superior results to the other models. This is attributed to the substantially larger data set size compared to the Southern trained models. Overall the tests provided a tool to assess the progress made in the investigation and allows for further improvements to be made.

Chapter 8

Discussion

8.1 LinkNet compared to previous Neural Networks

The choice of a LinkNet architecture was based on previous research on UNet [3]. Two Neural Networks were compared in this paper, UNet and DenseNet. The DenseNet models underperformed 67% of the time and presented a deterrent in favour of such Neural Networks implementing dense layers. Therefore, due to the high performance of the UNet model in both the Southern and Northern hemispheres, similar Neural Network architectures were sought out. LinkNet was one of these architectures among others. It's fair to say that the LinkNet model underperformed when compared to the UNet, CNN and even a few of the DenseNet models, with all of the UNet and CNN models providing an accuracy greater than 90% compared to LinkNet's best accuracy of 87.09%. This poor result in comparison to the aforementioned models could be attributed to the variation in training and test data implemented for each model. However, it is likely that this Neural Network architecture is not suited to this application and perhaps needed more time to optimise each layer. This optimisation could involve the inclusion of more dropout layers that will make the model learn patterns harder. This would in turn require the number of epochs to increase and consequently increasing the duration of the training process.

8.2 The Inclusion of Melting and Freezing Cycles

In understanding the research done in [3] and [7], these papers focused on creating Neural Network models based solely on SAR images retrieved from their particular data sources.

8.3. THE LACK OF DATA AUGMENTATION TECHNIQUES

This investigation aimed to utilise the information presented in these papers and expand the knowledge and research in the field of SIC estimation techniques. The expansion of this research entailed the inclusion of freezing and melting periods in the Southern and Northern hemisphere. The theory in including these seasonal cycles was based on the idea that because the Antarctic is known to have the most drastic change in land surface area of any geological piece of land, that the SIC's during each seasonal cycle would contain nuances that could perhaps implement hidden features of the sea ice contained in each region. An important note to make is that the models trained in the Southern region during the melting season provided the best performance. While this may be due to there being more southern data available during this period, it is unclear if the inclusion of this period had an effect on the models. Further research needs to be done where the same amount of data is implemented in a Neural Network model for both the freezing and melting period in the Southern hemisphere. Only in this investigation will we be able to conclude if the inclusion of seasonal cycles affected the SIC estimations with a positive outcome. For now, the inclusion for Southern melting data provides the best performance in this particular investigation.

8.3 The Lack of Data Augmentation Techniques

The decision to exclude data augmentation techniques was based on research conducted on the CNN, UNet and DenseNet models [3]. In all cases of training and testing, the models that implemented data augmentation techniques performed worse. This could be caused by the models overfitting in the training process. The addition of including data augmentation is always approached when solving a problem that lacks extensive data sources. However, relying on data augmentation should not be the sole focus of any investigation as there are downsides to its implementation. This investigation did not include any data augmentation techniques but a different approach can be to test its effectiveness using alternative data augmentation methods that resolve the overfitting issue in current SIC estimation models.

8.4 The Approach to Transfer Learning

Transfer learning is a popular approach in machine learning that is based on the idea of training on an initial set of data and storing that knowledge, then continuing training on another set of data with similar features as the first data set. Just like data augmentation,

it aims in solving the issue regarding the minimal amount of SIC data in the Southern hemisphere. Transfer learning in previous research [3] provided some interesting results in terms of performance. Using transfer learning (North then South) in the CNN models provided better results when compared to the Southern only trained CNN models. In the case of UNet, the transfer learning and standard learning models produced almost identical results. However, in the DenseNet model, the transfer learning model outperformed the standard learning model by a large margin. This resulted in a DenseNet model that was previously deemed invalid based on the large error now in contention when deciding which Neural Network to implement. This is interesting as it seems that the transfer learning approach greatly improves models based on architectures containing dense layers.

In this investigation the opposite occurred, all the models trained with the transfer learning approach produced the worst performance in terms of error. This is most likely due to an error in the training process conducted on the Google Colab coding platform. When training, the loss in the initial stage decrease as expected, but as the second stage began training, the loss spiked and essentially retrained the model and produced poor results due to the volatile training process. There is a possible workaround solution as this issue was probably caused by incorrectly loading the model.

8.5 User Requirements

The final point of discussion pertains to the predefined user requirements presented in Table 3.1. These requirements essentially outlined the progress of this investigation and ultimately determines if the investigation was a success. Overall, the final models produced predictions with high spatial and temporal resolution. Although the models do not meet the accuracy requirements, the predictions produced are satisfactory due to the accuracy being marginally close to the required specification. The models are able to produce SIC estimations in a timely manner for both the Arctic and Antarctic region. And focusing on the acceptance tests, the two tests that failed could be corrected with more time given. Thus the produced models created with the user requirements are satisfactory.

Chapter 9

Conclusions

This investigation aimed to develop a SIC estimation model with high performance in the Southern hemisphere region containing the Antarctic Circle. The LinkNet Neural Network architecture as well as a Convolutional AutoEncoder architecture was chosen to be implemented. During the training process, the AutoEncoder models were disregarded as viable options to consider, this was due to the models' inability to display their predictions in a manner that meets the visual assessment criteria. AutoEncoders are often used as tools for the compression of images, this is also a plausible cause for the invalidity of the AutoEncoder models in question.

The loss for each LinkNet model was defined by the uncertainty weighted mean absolute error (UW MAE). An important observation is made that indicates that models trained on the Southern hemisphere during its melting period, produces the best results in terms of accuracy and visual assessment. As mentioned before, this is likely due to more images available in the melting period than compared to the freezing period. Another observation to be made is that the models trained on Northern hemisphere, although containing more image data, was unable to surpass the Southern melting trained models with fewer image data. This result enforces the evidence there is a clear distinction in the SIC's present in the Northern hemisphere compared to the Southern hemisphere. The evidence of this result poses an interesting question; Do these large sea ice landmasses contain any other hidden information that can be used in implementing a SIC model?

As a final note, it is important to mention the excellent efficacy of models trained using Neural Network architectures like LinkNet and UNet. Both these models intended for image segmentation were easily adapted for SIC estimations and achieved its purpose with high performance.

Chapter 10

Recommendations

10.1 Alternative Neural Networks

With the high performance of architectures like LinkNet and UNet, similar networks could be implemented in the future. A few alternative Neural Networks present potential architectures to be implemented, namely, PSPNet (Pyramid Scene Parsing Network), DeepLabV3 and FPN (Feature Pyramid Network). These networks are common in the implementation of image segmentation algorithms, but like the models in this investigation, they can be adapted for a specific use.

Due to the limitations of Google Colab, certain Neural Networks could not be implemented. This was because unlike LinkNet and UNet the images were not downsampled then upsampled in the layer of the network. Google Colab runs out of RAM when loading large batches for training as well as when the images are not downsampled. By making use of Google Colab Pro or porting to Google Cloud Platform (which is a platform focused on machine learning), a variety of alternative Neural Network architectures are open to being explored.

10.2 Transfer Learning

Neural Network architectures that are based on adding dense layers as well as architectures that don't downsample then upsample images, stand to benefit from the transfer learning approach. Perhaps training each model for a higher number of epochs will work due to

the loss spike during the second stage of the transfer learning process.

10.3 Increase Image Dimension

The SAR images used in this investigation were downsampled to 128x128 pixels. These images were used to train and test every Neural Network model in this investigation. By increasing the input dimensions of the SAR images fed into each Neural Network model to 256x256 pixels, the model will have more information and able to produce better predictions.

10.4 Alternative Data Sources

Although there is limited access to ground truth data in the Southern hemisphere more could be found. There are plenty of sea ice concentration images and other information related to sea ice available online, the NSIDC, in particular, is home to a large number of these products that could be made use of in this investigation. These products source SIC's via a variety of different remote sensing instrumentation. This information coupled with the increased image dimension poses a promising SIC model.

Bibliography

- [1] National Oceanic and Atmospheric Administration, “How does sea ice affect global climate?,” *Natl. Ocean Serv.*, vol. 2018, pp. 1–3, 2018, Accessed: Nov. 11, 2020. [Online]. Available: <https://oceanservice.noaa.gov/facts/sea-ice-climate.html>.
- [2] C. Eayrs, D. Holland, D. Francis, R. Kumar, T. Wagner, and X. Li, “Antarctic Seasonal Sea Ice Melts Faster Than It Grows - Eos,” *Eos*, 2019. [Online]. Available: <https://eos.org/editors-vox/antarctic-seasonal-sea-ice-melts-faster-than-it-grows>.
- [3] S. Dominicus, ”Sea Ice Concentration Estimation Techniques Using Machine Learning”, UCT, 2019
- [4] “National Snow and Ice Data Center,” *Choice Rev.* Online, vol. 50, no. 02, pp. 50-0899-50-0899, 2012, doi: 10.5860/choice.50-0899.
- [5] CMEMS, ”GLOBAL OCEAN ARCTIC AND ANTARCTIC - SEA ICE CONCENTRATION, EDGE, TYPE AND DRIFT (OSI-SAF)” https://resources.marine.copernicus.eu/?option=com_csw&view=details&product_id=SEAICE_GLO_SEAICE_L4_NRT_OBSERVATIONS_011_001.
- [6] Copernicus, “Copernicus Open Access HUB.” <https://scihub.copernicus.eu/dhus/#/home>.
- [7] J. Chi and H. C. Kim, “Prediction of Arctic sea ice concentration using a fully data driven deep neural network,” *Remote Sens.*, vol. 9, no. 12, 2017, doi: 10.3390/rs9121305.
- [8] C. O. Dumitru, V. Andrei, G. Schwarz, and M. Datcu, “Machine learning for sea ice monitoring from satellites,” *Int. Arch. Photogramm. Remote Sens. Spat. Inf. Sci. - ISPRS Arch.*, vol. 42, no. 2/W16, pp. 83–89, 2019, doi: 10.5194/isprs-archives-XLII-2-W16-83-2019.
- [9] W. Shibui, “GitHub - shibuiwilliam/Keras_Autoencoder: Autoencoders using Keras.” https://github.com/shibuiwilliam/Keras_Autoencoder.

BIBLIOGRAPHY

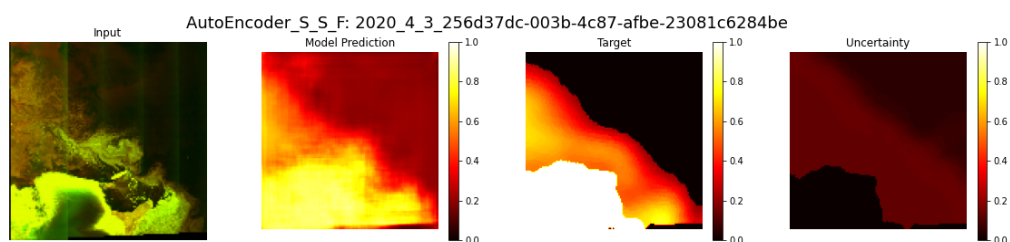
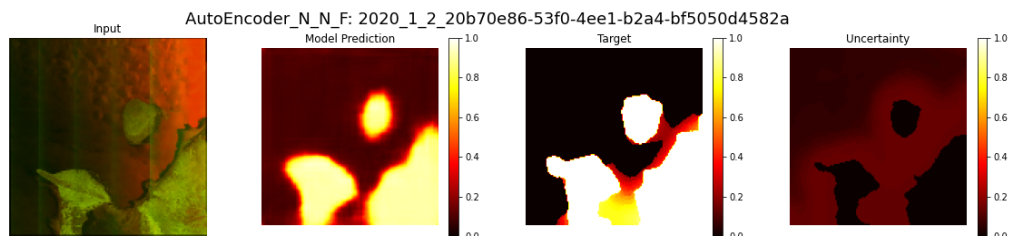
- [10] A. Chaurasia and E. Culurciello, “LinkNet: Exploiting encoder representations for efficient semantic segmentation,” in *2017 IEEE Visual Communications and Image Processing, VCIP 2017*, 2018, vol. 2018-Janua, pp. 1–4, doi: 10.1109/VCIP.2017.8305148.
- [11] L. Zhou, C. Zhang, and M. Wu, “D-linknet: Linknet with pretrained encoder and dilated convolution for high resolution satellite imagery road extraction,” in *IEEE Computer Society Conference on Computer Vision and Pattern Recognition Workshops*, Dec. 2018, vol. 2018-June, pp. 192–196, doi: 10.1109/CVPRW.2018.00034.
- [12] M. WU, C. ZHANG, IEEE Member, J. LIU, L. ZHOU, and X. LI, “Towards Accurate High Resolution Satellite Image Semantic Segmentation,” IEEE Xplore. <https://ieeexplore.ieee.org/stamp/stamp.jsp?arnumber=8700168>.
- [13] N. Hitsai, “GitHub - nickhitsai/LinkNet-Keras: implementation of LinkNet in Keras,” GitHub, Sep. 29, 2017. <https://github.com/nickhitsai/LinkNet-Keras>.

Appendix A

Neural Network Predictions

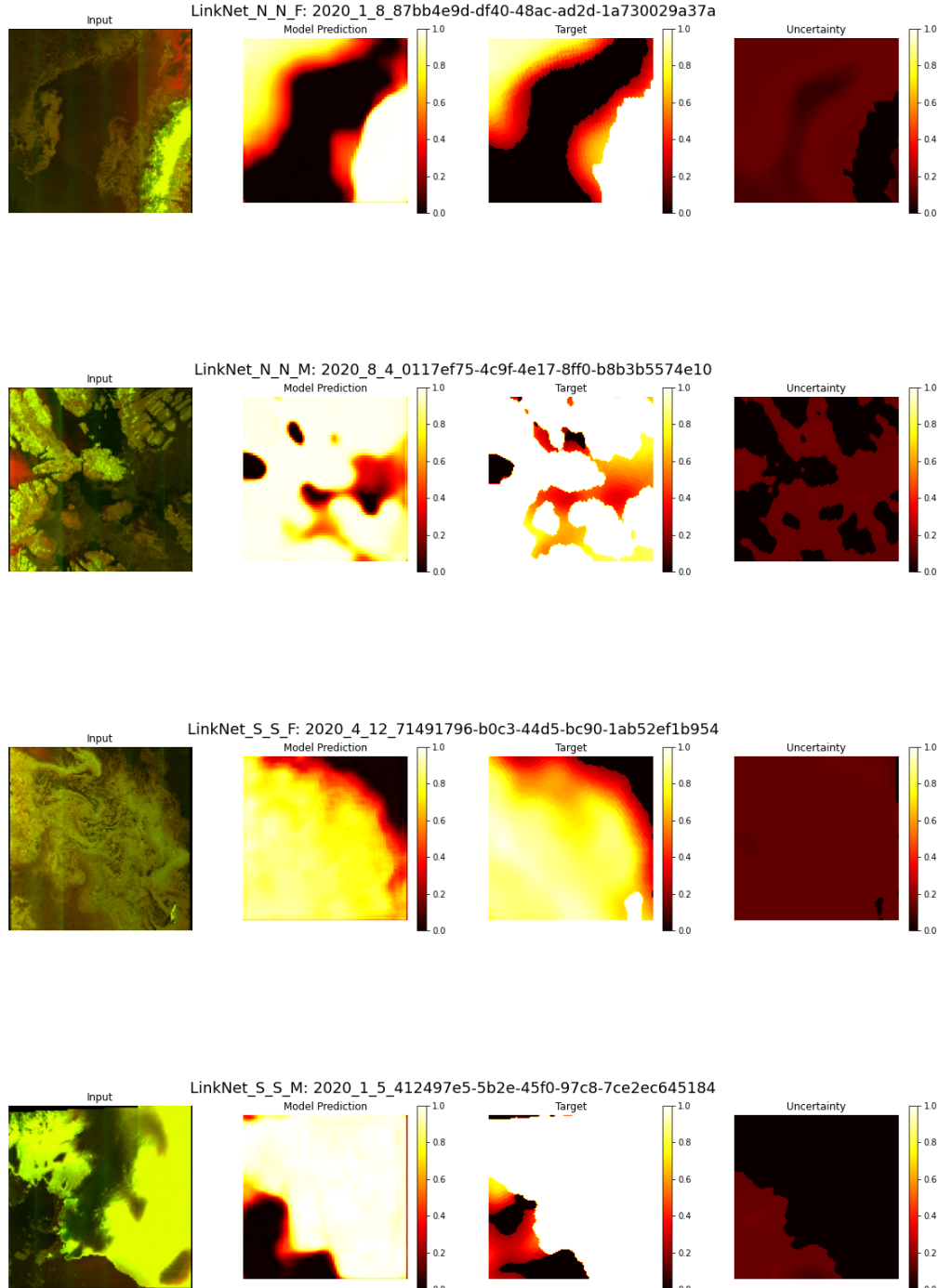
A.1 AutoEncoder Predictions

A.1.1 Arbitrary Locations

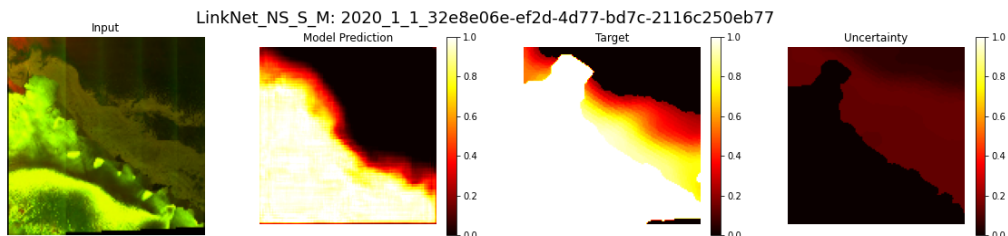
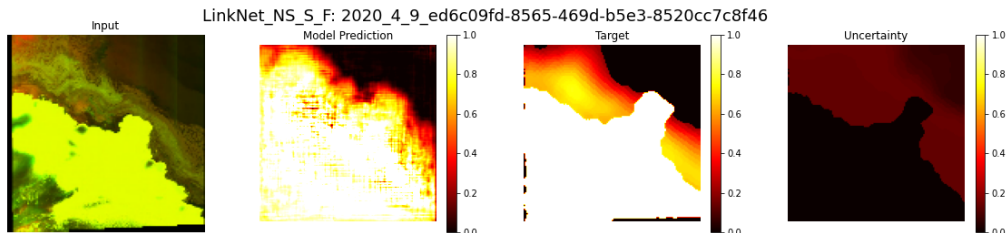


A.2 LinkNet Predictions

A.2.1 Arbitrary Locations

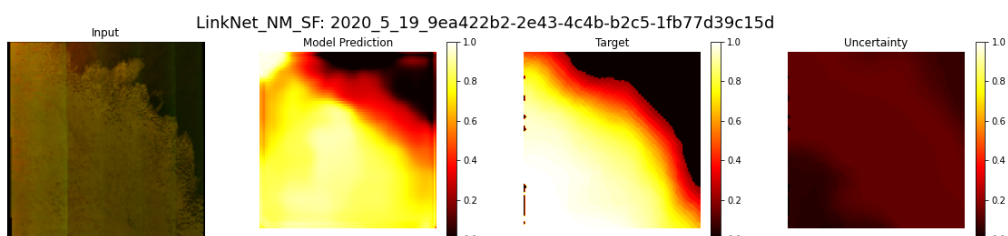
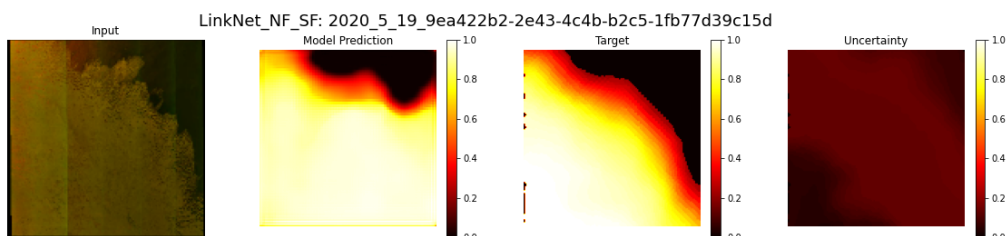


A.2. LINKNET PREDICTIONS

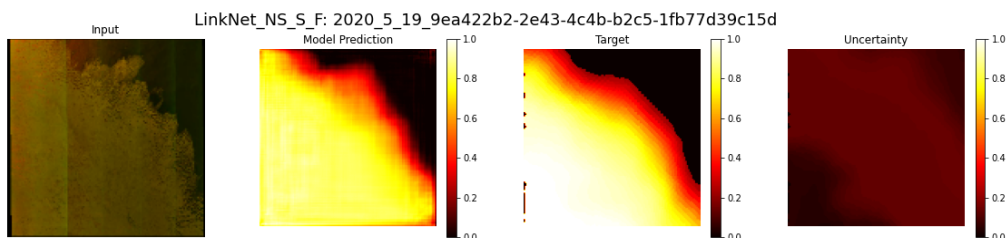
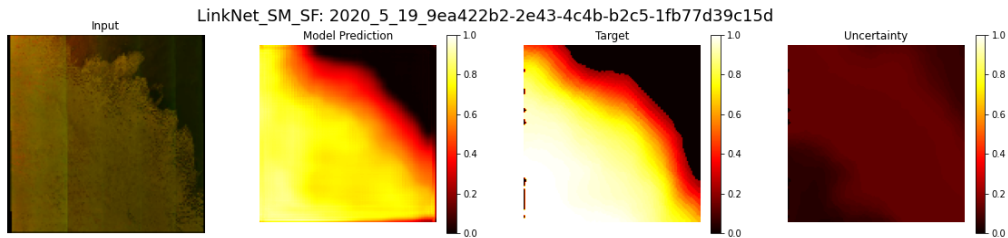
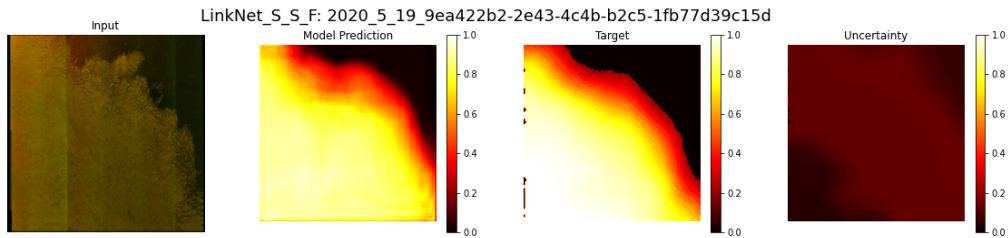


A.2.2 Specific Locations in the Antarctic Region

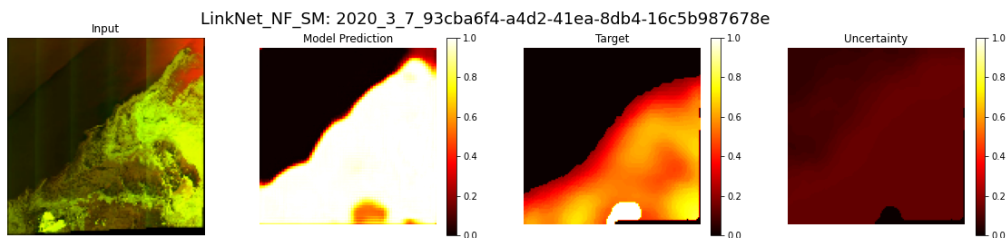
Freezing Period



A.2. LINKNET PREDICTIONS



Melting Period



A.2. LINKNET PREDICTIONS

